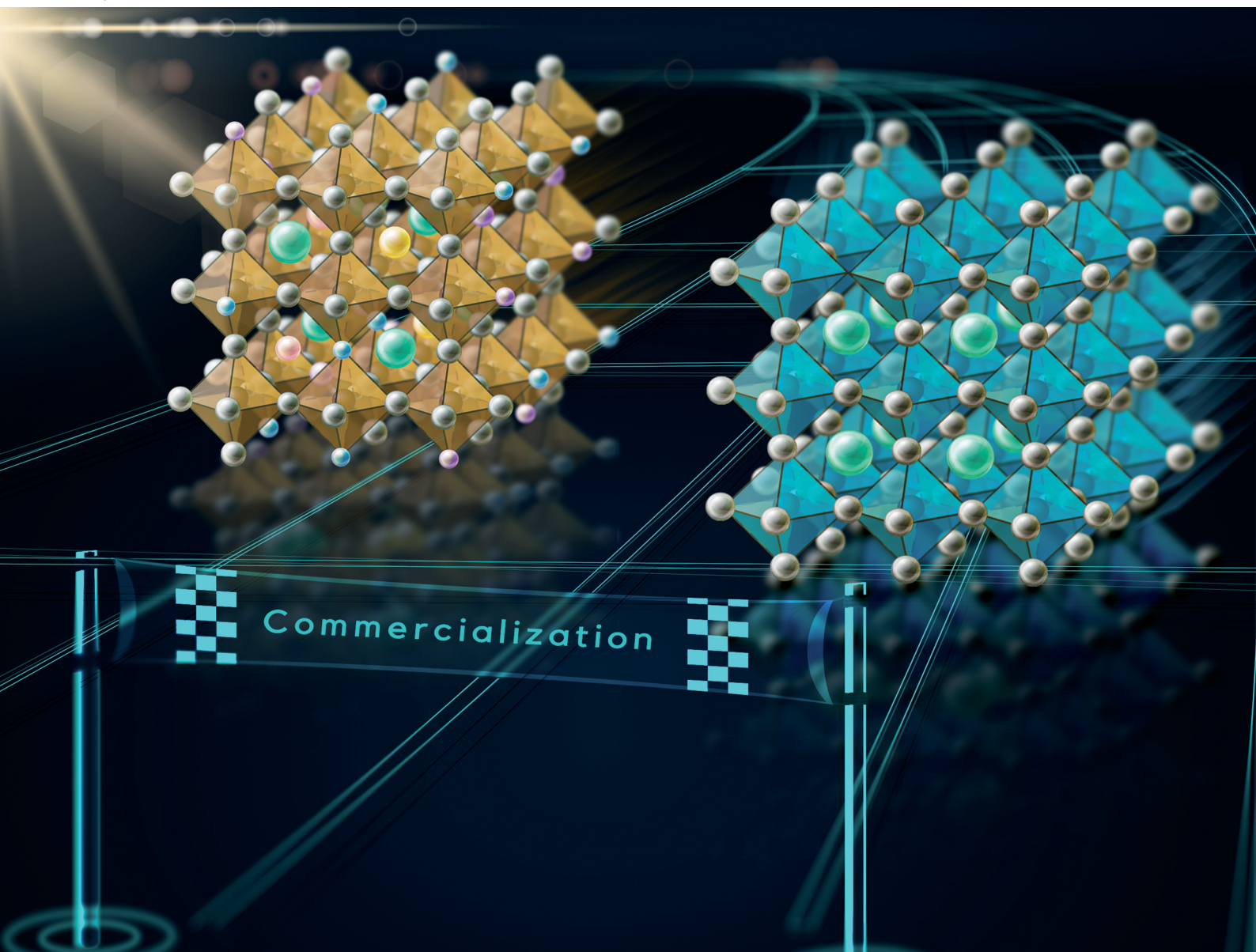


Journal of Materials Chemistry C

Materials for optical, magnetic and electronic devices

rsc.li/materials-c



ISSN 2050-7526

PERSPECTIVE

Mojtaba Abdi-Jalebi *et al.*

The race between complicated multiple cation/anion compositions and stabilization of FAPbI_3 for halide perovskite solar cells



Cite this: *J. Mater. Chem. C*, 2023, 11, 2449

The race between complicated multiple cation/anion compositions and stabilization of FAPbI_3 for halide perovskite solar cells

Quanyao Lin, ^a Dominik J. Kubicki, ^b MirKazem Omrani, ^a Firoz Alam^c and Mojtaba Abdi-Jalebi ^a

Compositional modifications and passivating additives have been key enablers to achieve operationally stable halide perovskite devices with excellent optoelectronic properties. The thermal and structural instability of the most desirable single-cation metal halide perovskites motivates the use of multiple cation and mixed-halide compositions that indeed lead to superior optoelectronic and photovoltaic properties over the course of the development. The application of multiple cation/anion and additive-based alloyed perovskites could, however, be hindered by the formation of non-perovskite phases and bandgap increase. Recent studies have shown that exceptional performance can be achieved using simpler compositions, such as FAPbI_3 , with appropriate passivation methods. In this perspective, we will present the current status of multiple cation/anion perovskites and discuss the role of common monovalent cations such as FA, MA, Cs, Rb, and K on the stability, optoelectronic properties, and charge transport behavior of lead halide perovskites. We further present the common stabilization and passivation strategies for phase-pure FAPbI_3 . We highlight the key role of solid-state NMR in determining the atomic-level mechanism of action of the various dopants and passivation agents. We then summarize the current understanding of the benefits and drawbacks of the cation alloying approach relative to the passivated phase-pure FAPbI_3 . Finally, we discuss the perspective for future research directions to achieve stable perovskite solar cells that approach the theoretical limit.

Received 25th October 2022,
Accepted 18th December 2022

DOI: 10.1039/d2tc04529j

rsc.li/materials-c

^a Institute for Materials Discovery, University College London, Malet Place, London, WC1E 7JE, UK. E-mail: m.jalebi@ucl.ac.uk

^b Department of Physics, University of Warwick, Coventry, CV4 7AL, UK

^c Department of Electronic and Electrical Engineering, University College London, London, WC1E 6BT, UK



Quanyao Lin

Quanyao Lin is currently a PhD student at the Institute for Materials Discovery (IMD), University College London (UCL). He received his MPhil from the University of Cambridge in 2019 and his BEng in Materials Science & Engineering from Imperial College London in 2018. His current research interest is focused on developing novel approaches for efficient, cost-effective, and environmentally friendly perovskite-based photovoltaic devices.



Dominik J. Kubicki

Dr Dominik J. Kubicki has been an Assistant Professor in the Department of Physics at the University of Warwick (UK) since September 2021. He graduated from the Warsaw University of Technology (Poland) in 2013 and completed his PhD at EPFL (Switzerland) in 2018. He held a Marie Curie-Skłodowska Fellowship at the University of Cambridge (UK) from 2018 to 2021. His research focuses on new materials for sustainable optoelectronic technologies.



contender for traditional semiconductors for their use in optoelectronic devices such as solar cells and light-emitting diodes.¹ In contrast to conventional semiconductors such as c-Si, inexpensive perovskites are easily modifiable to achieve the desired properties and offer simple bandgap tunability and low-temperature solution-processability, thus enabling low-cost depositions such as roll-to-roll printing onto lightweight and bendable substrates.² In addition, they have moderate defect densities yet retain excellent bulk optoelectronic properties including strong light absorption and long photogenerated charge carrier diffusion lengths. This, in turn, facilitates efficient charge transport, which results in a power conversion efficiency (PCE) of 25.7%³ in single-junction perovskite solar cells (PSCs) through changes in materials composition,



MirKazem Omrani

group, led by Dr Mojtaba Abdi-Jalebi, at UCL as a visiting researcher. His current research interests involve using cost-effective carbon materials to achieve efficient perovskite-based flexible optoelectronic devices.



Firoz Alam

semiconducting nanomaterials, mixed cation/halide perovskites and fabrication of emerging solar cells. He has published over 30 peer-reviewed research articles in internationally reputed journals and is a full member of the Royal Society of Chemistry, UK.

processing conditions, interface engineering, anion engineering and device architectures with ultra-low-cost fabrication *via* low-temperature solution processes.^{4,5} Furthermore, perovskite light-emitting diodes are achieved with external quantum efficiencies of over 23%.⁶ Recently next-generation perovskite-silicon tandem solar cells have achieved a new record efficiency value of 32.5% and have been documented in the NREL charts.³ However, the long-term stability of the perovskite devices against light, humidity, and heat remains a pressing challenge that hinders their commercialization and requires further understanding of the optoelectronic properties of metal halide perovskite devices and of how they can be controlled further with materials chemistry and device architecture optimization.⁷ To address this challenge, chemical modification⁸ and different passivation approaches^{9,10} have been intensively studied. This includes the substitution of cations and anions in the perovskite structure, most generally denoted as ABX_3 , that comprises at least one monovalent cation, methylammonium ($(CH_3NH_3)^+$ or MA^+), formamidinium ($(CH(NH_2)_2)^+$ or FA^+), cesium (Cs^+), rubidium (Rb^+), potassium (K^+) at the A-sites, a divalent metal, lead (Pb^{2+}) at the B-sites and halides, chlorine (Cl^-), bromine (Br^-), or iodine (I^-) at the X-sites.

Since the first implementation of perovskite materials in photovoltaic devices,¹¹ methylammonium lead iodide ($MAPbI_3$) has been the most widely studied material for perovskite solar cells (PSCs).¹² However, the thermal instability and significant moisture sensitivity of this material have motivated the research community to alter the A-site cation.^{13,14} Formamidinium lead iodide ($FAPbI_3$) has emerged as a promising alternative with its higher thermal, moisture, and photostability from the relatively inert formamidinium proton. Additionally, the replacement of the MA cation in $MAPbI_3$ with a slightly larger FA cation in $FAPbI_3$ decreases the optical bandgap from 1.52 to 1.45 eV, due to changes in the cation radius, which allows absorption of photons over a broader solar spectrum.^{13,15}



Mojtaba Abdi-Jalebi

Dr Mojtaba Abdi-Jalebi is an Assistant Professor in Energy and Functional Materials in the Institute for Materials Discovery, University College London. He completed his PhD in Physics at Cavendish Laboratory, University of Cambridge. From 2018 to 2020, he was a Junior Research Fellow at Wolfson College in Cambridge. His research focuses on the development of emerging semiconductors for low-cost optoelectronic and electrochemical devices for low-cost electronics applications and energy systems enabling carbon capture and production of solar fuels. His research aims to develop and incorporate new inexpensive materials in energy devices to alter the energy landscape by reducing the cost of energy production, consumption, and storage.



It is well known in the literature that FAPbI_3 crystallizes into two polymorphs: (i) the black cubic perovskite phase (α -phase) with space group $Pm\bar{3}m$; and (ii) the yellow non-perovskite hexagonal phase (δ -phase) with space group $P6_3mc$.^{16,17} However, the thermodynamically stable form of pure formamidinium lead iodide at room temperature is a non-photoactive yellow polymorph (δ -phase), which is formed preferentially owing to the cation size mismatch, and which is essentially not usable for optoelectronic purposes.⁸ The most extensively studied method to stabilize the photoactive black phase (α -phase) of FAPbI_3 is by partial substitution of FA^+ with MA^+ and/or Cs^+ to form mixed-cation perovskites.^{18,19} Perovskite solar cells (PSCs) based on these compositions with average PCEs exceeding 20% and characterized by long-term stability have been widely reported.¹⁸ So far, the most reproducible and stable compositions with superior optoelectronic properties for state-of-the-art single junction PSCs for outdoor applications include mixtures of MA/FA ,^{8,13} FA/Cs ,²⁰ and Cs/MA/FA ,¹⁸ with lead on the B-site and often a mixture of halides (I^- , Br^- , and Cl^-) on the X-site. Other monovalent alkali cations, including Li^+ ,²¹ Na^+ ,²² K^+ ,²³ and Rb^+ ,²⁴ have been studied as perovskite additives and suggested to occupy various locations in the structure.²⁵ In particular, potassium (K) and rubidium (Rb) have been widely used as effective additives in order to achieve superior optoelectronic properties in halide perovskites.^{23,24}

However, recently there has been a trend of moving towards simpler perovskite compositions, particularly FAPbI_3 , whereby the stability of the black photoactive polymorph is achieved through more subtle means than direct A-site cation and halide mixing, although most reports still required a small amount of MA and other alloying cations to be introduced. These methods include the addition of reagents such as methylammonium chloride (MACl) combined with formamidinium formate (FAFa),⁵ methylammonium thiocyanate (MASCN),²⁶ methylammonium formate (MAFa),²⁷ methylenediammonium (MDA),²⁸ and cesium ions.²⁹ These strategies have been very successful leading to PCEs of up to 25.7% (certified 25.4%) in the case of FAPbI_3 made in the presence of MACl.³⁰ Very recently, a new strategy has been proposed that does not use MA or any other cations that are incorporated into the perovskite structure. Doherty *et al.* used ethylenediaminetetraacetic acid (EDTA) and showed that it stabilizes the black perovskite phase of FAPbI_3 by templating its growth from solution in a way that leads to a slight octahedral tilt, with the highly disordered EDTA molecules being attached to the grain surface of the resulting solid.³¹ Fig. 1a summarizes the performance of the state-of-the-art PSCs based on both FAPbI_3 and mixed-cation perovskites. These recent developments raise the question of whether using complex multiple cation/anion compositions is truly necessary for achieving high-performance and stable photovoltaic devices.

To answer this question, in this perspective, we first evaluate the impact of common monovalent cations, including MA^+ , FA^+ , Cs^+ , Rb^+ , and K^+ , on the phase stability, optoelectronic properties and charge transport behavior in the context of photovoltaic application. We highlight the use of solid-state

NMR as a quantitative atomic-level probe capable of identifying where the dopants are located in the resulting material. Following that, we discuss some common strategies to achieve stabilization of the black α - FAPbI_3 phase, highlighting the atomic-level mechanism of stabilization where it is known. Finally, we evaluate the advantages and limitations of multiple cation/anion perovskite systems and phase-pure FAPbI_3 for photovoltaic applications and give an outlook on the future directions of developing perovskite materials for highly efficient PSCs with long-term stability.

2. Role of monovalent cations in metal halide perovskites

2.1 Predicting the stability of perovskite phases

For 3D perovskites, the ABX_3 crystal structure consists of corner-sharing $[\text{BX}_6]^{4-}$ octahedra structurally stabilized by monovalent A cations located in $[\text{AX}_{12}]$ cubo-octahedra (Fig. 1b). The size of the monovalent cations influences the bond lengths and angles with the adjacent octahedra and therefore has a direct impact on the crystal symmetry and phase stability. The formation and stability of an arbitrary perovskite structure can be estimated phenomenologically using the Goldschmidt tolerance factor (t): $t = (r_{\text{A}} + r_{\text{X}}) / [\sqrt{2}(r_{\text{B}} + r_{\text{X}})]$, where r_{A} , r_{B} , and r_{X} are the ionic radii of the A, B and X components. In stable perovskite structures, the Goldschmidt tolerance factor is empirically observed to take values $0.8 < t < 1.0$. For lead-based perovskites, FA^+ , MA^+ and Cs^+ lead to values that fit within this range, with MAPbI_3 at $t = 0.91$, FAPbI_3 at $t = 0.99$, and CsPbI_3 at $t = 0.80$,³² as shown in Fig. 1c. Notably, the two latter structures have tolerance factors at the limit of the stability threshold and are experimentally observed to be unstable at room temperature. They transition to δ - FAPbI_3 and δ - CsPbI_3 , respectively, which are both yellow hexagonal (non-perovskites) polymorphs. In contrast, considering the smaller ionic radius of Rb^+ (152 pm) compared to Cs^+ (167 pm), RbPbI_3 ($t = 0.78$) only forms a yellow hexagonal polymorph at room temperature with no phase transformation until its melting point, therefore is not suitable as a light absorber material for PSCs.³³

The α -to- δ phase transition in FAPbI_3 is especially exacerbated in the presence of humidity and thermal stress.⁴⁴ Partial substitution of FA^+ with the smaller MA^+ reduces the average t value and the strain in the lattice structure, achieving cubic phase stabilization at room temperature. Pellet *et al.* first showed that MA-FA mixing leads to the stabilization of the black perovskite phase.⁴⁵ Later on, Binek *et al.* showed that the black perovskite phase was stabilized at room temperature with as little as 15% MA content.⁴⁶ In addition, the authors have tentatively suggested that owing to the large dipole moment of MA, its addition reduces the formation energy for FA/MA perovskites, improves the moisture stability of FAPbI_3 and inhibits phase separation.^{46,47} PSCs based on different compositions ($\text{FA}_{1-x}\text{MA}_x\text{PbI}_3$ or $\text{FA}_{1-x}\text{MA}_x\text{PbI}_{3-x}\text{Br}_x$, where $0 \leq x \leq 1$) demonstrated high crystallinity of the α -phase with greatly suppressed δ -phase and significantly improved device



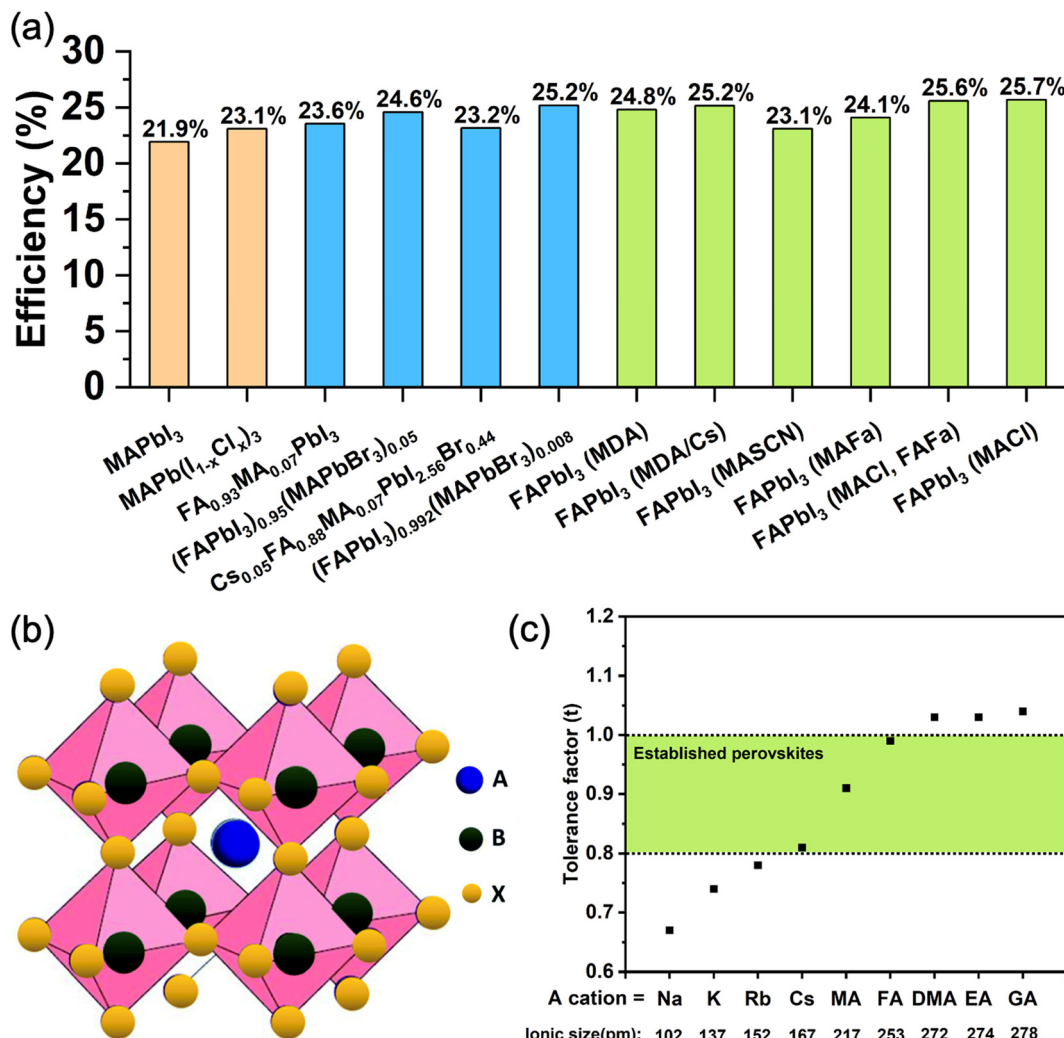


Fig. 1 (a) Summary of state-of-the-art lead halide PSCs based on MAPbI_3 ,³⁴ $\text{MAPb}(\text{I}_{1-x}\text{Cl}_x)_3$,³⁵ $\text{FA}_{0.93}\text{MA}_{0.07}\text{PbI}_3$,³⁶ $(\text{FAPbI}_3)_{0.95}(\text{MAPbBr}_3)_{0.05}$,³⁷ $\text{Cs}_{0.05}\text{FA}_{0.88}\text{MA}_{0.07}\text{PbI}_{2.56}\text{Br}_{0.44}$,³⁸ $(\text{FAPbI}_3)_{0.992}(\text{MAPbBr}_3)_{0.08}$,³⁹ $\text{FAPbI}_3(\text{MDA})$,⁴⁰ $\text{FAPbI}_3(\text{MDA/Cs})$,⁴¹ $\text{FAPbI}_3(\text{MASCN})$,²⁶ $\text{FAPbI}_3(\text{MAFa})$,²⁷ $\text{FAPbI}_3(\text{MACl, FAFa})$ ⁵ and $\text{FAPbI}_3(\text{MAC})$.⁴ (b) Schematic of the crystal structure of an ABX_3 metal halide perovskite.⁴² Reproduced with permission from ref. 42. Copyright © 2019, The Royal Society of Chemistry. (c) Calculated tolerance factor of APbI_3 perovskite with common monovalent cations (Na, K, Rb, Cs, MA, FA, DMA, EA, GA). The ionic radii are obtained from Kim *et al.*⁴³

efficiencies.^{45,48} However, since MA^+ forms a smaller number of hydrogen bonds with its adjacent ions, it is more volatile compared to FA^+ , resulting in decreased thermo- and photo-stability of perovskite films. Phase stabilization of $\alpha\text{-FAPbI}_3$ with the more thermally stable Cs^{+49-51} and $\text{Rb}^{+52,53}$ was therefore developed. The inorganic Cs^+ and Rb^+ have a much smaller ionic radius than FA^+ , providing improved interaction between FA^+ and I^- and enabling structural stability of FAPbI_3 without the aid of MA^+ or Br^- while also enhancing the environmental stability of the materials.^{50,52} More complex mixed cation systems such as triple cation (FA/MA/Cs ¹⁸ or FA/MA/Rb ^{54,55}) and quadruple cation (FA/MA/Cs/Rb ⁵⁶) were also extensively studied and a substantially improved photo- and phase stability and resistance to halide-induced phase segregation were observed compared to their single- or double-cation counterparts, indicating a contribution of entropic stabilization to the system.⁵⁷

2.2 Where are the cations located? Speciation studies using solid-state NMR

To understand the microscopic role of cation dopants in halide perovskite compositions, it is essential to elucidate their speciation, that is to identify the phases in which they are present. Solid-state magic angle spinning (MAS) nuclear magnetic resonance (NMR) is perfectly suited to achieve this goal because it probes each of the cations separately, providing well-resolved peaks for species with different local environments. In practice, this means that cations present in different crystal structures (*e.g.*, Cs^+ in CsI , $\alpha\text{-CsPbI}_3$, $\delta\text{-CsPbI}_3$, and Cs^+ incorporated into the perovskite structure of FAPbI_3) each have a distinct peak shift which unambiguously and quantitatively identifies it in a mixture of phases. The use of solid-state NMR to study the speciation of dopants and other aspects of the atomic-level structure of halide perovskites has recently been reviewed.^{58,59}



The speciation of Cs^+ , Rb^+ , and K^+ in lead halide perovskite compositions has been elucidated using ^{133}Cs , ^{87}Rb , and ^{39}K solid-state NMR, respectively.^{60,61} Even before those studies, there was a general agreement that Cs^+ forms solid solutions with MA and FA in mixed-cation perovskites such as cesium-formamidinium (Cs/FA) and cesium-methylammonium-formamidinium (Cs/MA/FA) lead iodide-bromides. However, the role of the other cations such as Rb and K had been widely disputed. Kubicki *et al.* have shown using MAS NMR that Cs^+ is indeed incorporated into a variety of lead halide perovskites, but the same is not true for Rb^+ and K^+ .^{60,61} These two cations have been shown to phase segregate resulting in non-perovskite Cs/Rb- and Cs/K-rich phases. The formation of these phases necessarily led to the depletion of the photoactive perovskite phase of cesium. In addition, it has been suggested that this may simultaneously affect the I-to-Br ratio in the resulting perovskite. These two factors have been suggested as the key microscopic effects that lead to the structural and optoelectronic changes observed in Rb- and K-doped halide perovskites.^{60,61} Qualitatively similar results have been obtained using energy dispersive X-ray spectroscopy (EDS) and high-angle annular dark-field scanning transmission electron microscopy (HAADF STEM), although in those cases establishing the exact composition of the non-perovskite phases is more challenging.^{23,62} X-ray photoelectron spectroscopy measurements (XPS and HAXPES) did not show significant changes in the binding energies of the Pb 4f, I 3d and Br 3d core levels, further corroborating the result of no incorporation.⁶³ While the solid-state NMR results are unambiguous, they were obtained on materials made by mechanosynthesis under thermodynamic conditions. It is conceivable that under specific growth conditions, for example, controlled by growth kinetics, the speciation of that cation could be affected. Mishra *et al.* have recently shown this to be the case for Cs/dimethylammonium lead iodide perovskites.⁶⁴ In this context, two studies are noteworthy. Usiobo *et al.* have used nanoscale mass spectrometry imaging to study Cs, K, and Rb doped hybrid halide perovskites and found that, while Rb preferentially occupies grain boundaries as an Rb-rich, non-perovskite phase, there is also a detectable Rb signal originating from the perovskite grains.⁶⁵ Son *et al.* conducted a systematic study of K doping on the structural and optoelectronic properties of various hybrid halide perovskites and concluded that it leads to a substantial reduction in *J-V* hysteresis.⁶⁶ Those authors attributed the effect to potassium incorporation on the A site in the perovskite structure. Conversely, HAADF STEM results of a K-doped hybrid perovskite indicated that K is preferentially located at grain boundaries, with no detectable signal within the perovskite grains.²³ We suggest that more atomic-level studies are needed that compare materials made under different conditions (solid-state synthesis, thin films deposited without and with an antisolvent, thermal evaporation), to better understand how growth conditions affect the speciation of dopants. It is important to highlight that the compositional complexity resulting from phase segregation is conceivably one of the key factors determining the optoelectronic properties,⁶³ stability under ambient conditions^{56,63} and other types of time-dependent

changes (e.g., photobrightening and photodarkening).⁶⁷ The interplay between nanoscale phase composition and the resulting optoelectronic properties phenomena have been recently studied using spatially resolved electron microscopy techniques.^{68,69}

An important question is related to the detection limit of the various species in solid-state NMR, which as an analytical technique is characterized by intrinsically low sensitivity compared to optical spectroscopies. The ease with which the NMR signal is detected is dependent on the isotope of interest, and in the present case, it can be estimated that doping levels as low as *ca.* 0.1 mol% (for Cs, Rb) and *ca.* 1 mol% (for K) are viable for NMR studies.^{58,70} Table 1 summarizes the results on Cs, Rb, and K speciation derived from solid-state NMR in compositions most pertinent to optoelectronics research today. The overarching conclusions are that: (a) Cs, in general, incorporates into hybrid halide perovskites based on MA and FA, (b) Rb does not incorporate into halide perovskites based on MA and FA, (c) K does not incorporate into hybrid or all-inorganic perovskites, (d) attempts to incorporate Cs and Rb, or Cs and K simultaneously, lead to the formation of Cs/Rb and/or Cs/K non-perovskite phases which effectively reduce the amount of Cs in the perovskite structure. It is important to highlight that these studies have focused on the compositions most relevant to current solar cell research, and while they lead to useful general conclusions about the underlying chemistry, there still remain unexplored areas in the phase diagrams characterizing the multicomponent halide perovskites. Some examples include the formation of Cs-MA solid solutions of the type $\text{Cs}_x\text{MA}_{1-x}\text{PbI}_3$, incorporation of Rb into all-inorganic halide perovskites (CsPbX_3), incorporation of Cs, Rb, and K to hybrid halide perovskites with lower dimensionalities (2D/3D) and into compositions containing substantial amounts of chloride on the X-site.

There is scope for substantially decreasing the NMR detection limit in these cases by applying signal-enhancing strategies, such as MAS dynamic nuclear polarization (DNP).⁷¹ Some work has been done exploring these concepts but effective application of MAS DNP to a wide range of halide perovskite materials has a tantalizing potential and is yet to be realized.^{70,72} Very recently, MAS DNP has been demonstrated for the first time on an organic passivation layer in a single perovskite thin film with the total amount of passivation agents within the sample estimated to be 6 μg .⁷³ One of the areas where MAS DNP could be particularly insightful is the hypothesis that potassium ions passivate surface defects in hybrid halide perovskites, which is suggested to be their main mechanism of action.²³ MAS DNP has a unique capacity to enhance the sensitivity of surface NMR signals and, consequently, could be used to detect the hypothetical potassium species bound to perovskite surfaces. This approach may enable the detection of highly dilute species present at concentrations well below 0.01 mol%.

Another largely unexplored area is the use of solid-state NMR to study the speciation of other alkali and alkaline earth ions such as Li, Na, Mg, Ca, Sr, and Ba, which have also gained some prominence as dopants in halide perovskites but whose



Table 1 Incorporation and phase segregation of Cs^+ , Rb^+ and K^+ in lead halide perovskites from solid-state MAS NMR. The table is partly adapted with permission from ref. 79 and 80. Copyright © 2017, American Chemical Society

| Formal stoichiometry of perovskite composition | Incorporation into 3D lattice | | | Non-perovskite impurity phases | Related works exploring composition in devices |
|--|-------------------------------|----|---|---|--|
| | Cs | Rb | K | | |
| $\text{Cs}_x\text{FA}_{1-x}\text{PbI}_3$ ($x = 0.10, 0.15, 0.20, 0.30$) | ✓ | | | $\delta\text{-CsPbI}_3$ (for $> 10\%$ Cs) | As reported in <i>Adv. Energ. Mater.</i> 2015, 5, 1501310–1501318 (Lee <i>et al.</i>) ⁵⁰ |
| $\text{Cs}_{0.10}(\text{MA}_{0.17}\text{FA}_{0.83})_{0.9}\text{Pb}(\text{I}_{0.83}\text{Br}_{0.17})_3$ | ✓ | | | — | Triple cation composition as reported in <i>Energy Environ. Sci.</i> 2016, 9, 1989–1997 (Saliba <i>et al.</i>) ¹⁸ |
| $\text{Rb}_x\text{FA}_{1-x}\text{PbI}_3$ ($x = 0.05, 0.10$) | | ✗ | | $\delta\text{-RbPbI}_3$ | Similar to <i>Science</i> 2016, 354, 206–209 (mixed I/Br materials) ²⁴ |
| $\text{Rb}_{0.05}\text{MA}_{0.25}\text{FA}_{0.70}\text{PbI}_3$ | | ✗ | | RbPbI_3 | As above |
| $\text{Rb}_{0.05}\text{Cs}_{0.10}\text{FA}_{0.85}\text{PbI}_3$ | ✗ partial | ✗ | | $\text{Cs}_{1-x}\text{Rb}_x\text{PbI}_3$ | As above |
| $\text{Rb}_{0.05}\text{Cs}_{0.10}\text{MA}_{0.25}\text{FA}_{0.60}\text{PbI}_3$ | ✗ partial | ✗ | | $\text{Cs}_{1-x}\text{Rb}_x\text{PbI}_3$ | As above |
| $(\text{Rb},\text{Cs},\text{MA},\text{FA})\text{Pb}(\text{Br},\text{I})$ (non-stoichiometric) | ✗ partial | ✗ | | $\text{RbI}_x\text{Br}_{1-x}$ | quadruple cation composition as reported in <i>Science</i> 2016, 354, 206–209 (Saliba <i>et al.</i>) ²⁴ |
| $\text{K}_{0.10}\text{MA}_{0.90}\text{PbI}_3$ | | | ✗ | $\text{Cs}_{1-x}\text{Rb}_{1-x}\text{PbI}_{3-y}\text{Br}_y$, $\text{Rb}_x\text{Pb}_y\text{Br}_z$, KI , KPbI_3 | As reported in <i>J. Mater. Chem. A</i> 2017, 5, 7905–7911 (Zhao <i>et al.</i>) ⁸¹ |
| $\text{K}_{0.10}\text{FA}_{0.90}\text{PbI}_3$ | | | ✗ | KI , KPbI_3 | Not previously reported in PSCs |
| $\text{K}_{0.05}\text{MA}_{0.10}\text{FA}_{0.85}\text{PbI}_3$ | | | ✗ | KI , KPbI_3 | Not previously reported in PSCs |
| $\text{K}_{0.05}\text{MA}_{0.25}\text{FA}_{0.70}\text{PbI}_{2.75}\text{Br}_{0.25}$ | | | ✗ | KI , KBr | As reported in <i>Nano Energy</i> 2018, 45, 184–192 (Tang <i>et al.</i>) ⁸² and <i>J. Am. Chem. Soc.</i> 2018, 140, 1358–1364 (Son <i>et al.</i>) ⁸³ |
| $\text{K}_{0.05}\text{Cs}_{0.10}\text{FA}_{0.85}\text{PbI}_3$ | ✗ partial | | ✗ | KI , $\text{Cs}_{1-x}\text{K}_x\text{PbI}_3$ | Similar to <i>J. Am. Chem. Soc.</i> 2018, 140, 1358–1364 (Son <i>et al.</i>) ⁸³ and <i>Energy Environ. Sci.</i> 2017, 10, 2509–2515 (Bu <i>et al.</i>) ⁸⁴ (mixed I/Br materials) |
| $\text{K}_{0.075}\text{Cs}_{0.925}\text{PbI}_2\text{Br}$ | ✗ partial | | ✗ | $\text{Cs}_{1-x}\text{K}_x\text{I}_{1-y}\text{Br}_y$, $\text{Cs}_{1-x}\text{K}_x\text{PbI}_3$ | As reported in <i>Nano Lett.</i> 2017, 17, 2028–2033 (Nam <i>et al.</i>) ⁸⁵ |

atomic-level mechanism of action remains uncertain.⁵⁸ All these cations have NMR-active nuclei suitable for analogous speciation studies, albeit with varying degrees of experimental difficulty. For example, ^7Li and ^{23}Na are highly receptive and straightforward to implement, while ^6Li , ^{25}Mg , ^{43}Ca , ^{87}Sr , and $^{135/137}\text{Ba}$ are moderate to highly challenging owing to the combination of low natural abundance and large quadrupole moment, which leads to broad spectra. However, even in the most challenging cases, there exist protocols enabling NMR studies, which are greatly aided by high magnetic field instruments (> 20 T).⁵⁸ We suggest that atomic-level studies of their speciation are urgently needed since these cations have also been successfully used to modulate the optoelectronic performance of metal halide perovskites.^{74–78}

2.3 Enhancing optoelectronic properties of halide perovskite

2.3.1 Bandgap engineering *via* modification of A site cation. According to the detailed balance limit, a semiconductor should ideally have a bandgap of ~ 1.34 eV for an optimal PCE under full sun.⁸⁶ For lead halide perovskite, its band structure is determined by the divalent cation B and the halide X. The valence band edge originates from the strong antibonding coupling between the Pb 6s orbital and the I 5p orbital, whereas the conduction band edge arises from the bonding orbitals of Pb 6p.⁴³ On the other hand, the ionic bonding with the A-site cation is not located at the band edges and therefore has a less direct influence on the bandgap compared to the covalent interactions between the B-site and X-site ions. However, the cation influences the bandgap of the material indirectly by impacting the lattice straining or tilting the $[\text{BX}_6]^{4-}$ octahedra in the structure.⁸⁷ It has

been reported both computationally and experimentally that the bandgap of lead halide perovskite increases with smaller monovalent cations.^{20,88,89} Consequently, FAPbI₃ has a better bandgap for single-junction outdoor solar cells at 1.45 eV, compared to MAPbI₃ at 1.52 eV, due to its larger monovalent cation size that results in a higher symmetry of the cubic phase and a reduced bandgap,¹⁵ while replacing MA⁺ with Cs⁺ increases the bandgap to 1.73 eV.⁹⁰ Fig. 2a shows the bandgap energy for a range of common perovskite materials.

Partial substitution of monovalent cations also exhibits similar effects. Syzgantseva *et al.* have performed a computational study comparing the influence of MA⁺, Cs⁺, and Rb⁺ monovalent substitution on the properties of the doped FAPbI₃ system. The authors reported that the absorption spectra for doped FAPbI₃ exhibit a blue shift of the order of 0.1–0.2 eV observed in all the cases, where MA⁺ doped FAPbI₃ provides a slightly better onset compared to Cs⁺ and Rb⁺.⁹² The observed blue shift increases monotonically with dopant concentration and is more pronounced in the case of Rb⁺. These computation findings are consistent with experimental reports, according to which Cs⁺ and Rb⁺ incorporation increases the bandgap.^{18,33,93} A similar trend was observed by Prasanna *et al.* for FA_{1-x}Cs_xPbI₃ (Fig. 2b).⁹¹ Surprisingly, they also reported that substitution of FA with Cs in tin-based perovskite, where cesium cation is smaller than formamidinium cation, does not increase the bandgap of tin iodide perovskite, but steadily decreases it, contrary to what is observed for lead-based perovskite. Accordingly, they concluded that the change in bandgap energy of a particular perovskite composition is inversely related to the B–X orbital overlap. For FAPbI₃, upon



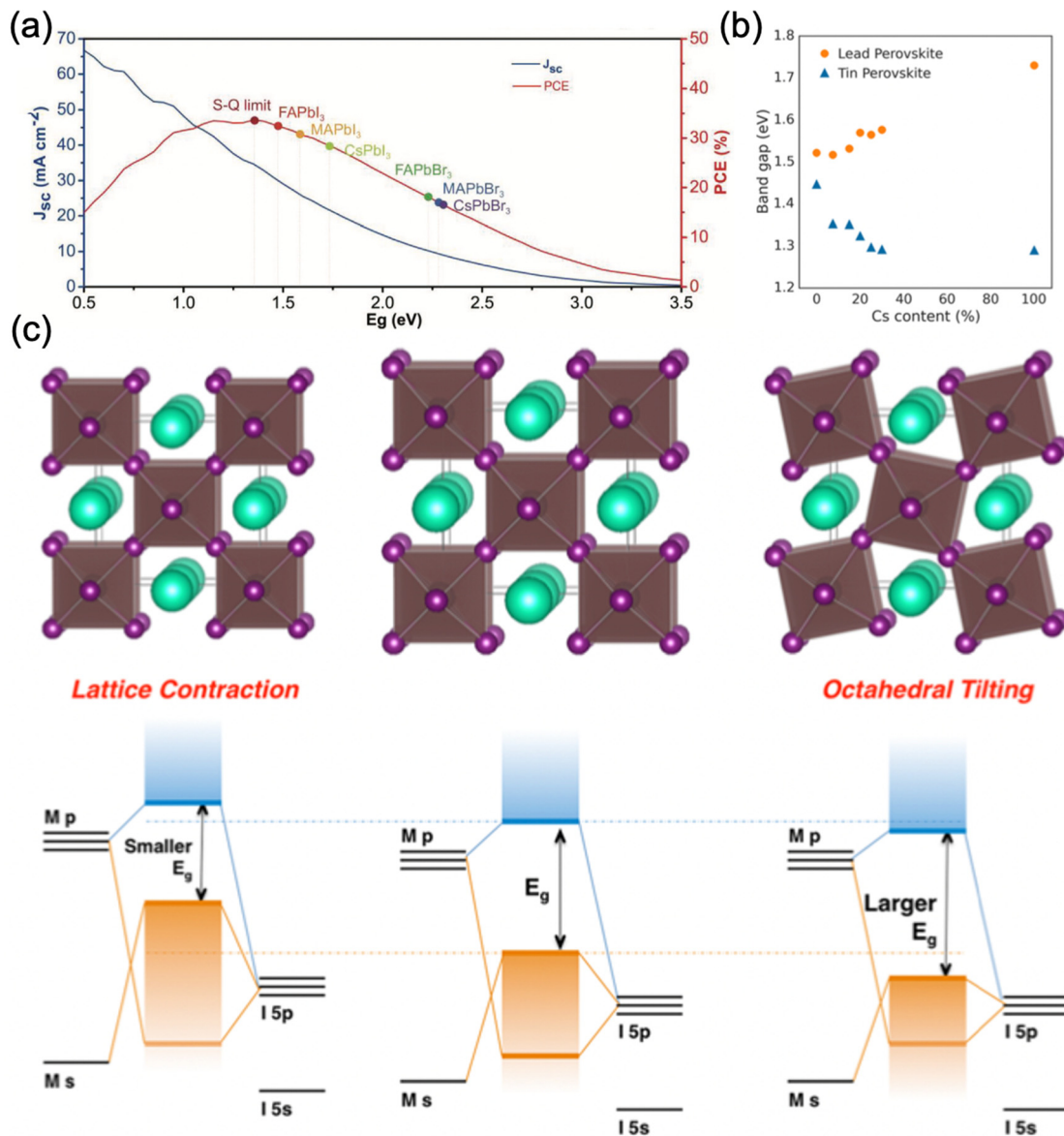


Fig. 2 Effect of A-site cation on the perovskite bandgap. (a) The theoretical efficiency and short-circuited current (J_{sc}) of various perovskite compositions compared to the detailed balance limit. Reproduced with permission from ref. 90. Copyright © 2022, WILEY-VCH Verlag GmbH & Co. KGaA, Weinheim. (b) Bandgap energy of Pb- and Sn-based perovskites $\text{FA}_{1-x}\text{Cs}_x\text{Ml}_3$ ($\text{M} = \text{Pb, Sn}$) with varying Cs content. (c) Relationship between lattice distortion (contraction and tilting) and the energy levels of the perovskite. (b) and (c) are reproduced with permission from ref. 91. Copyright © 2017, American Chemical Society.

partial Cs substitution, the FAPbI_3 crystal structure changed from cubic to tetragonal by tilting the PbI_6 octahedra to compensate for the change in perovskite lattice, as supported by synchrotron X-ray diffraction (XRD) measurements. This tetragonal distortion reduces the B-X-B bond angle and consequently reduces the extent of overlap between the metal and halide orbital, resulting in an increase in bandgap energy. Meanwhile, the XRD results showed that tin-based perovskites retained their cubic structure during the cesium substitution, with no octahedral tilting. The incorporation of Cs induced a reduction in the cubic unit cell size and therefore an increase in metal-halide orbital overlap, which subsequently decreased the bandgap energy (Fig. 2b and c).

More recently, oversized ($t > 1$) ammonium cations (e.g. methylenediammonium (MDA), guanidinium (Gua), and acetamidinium (Ace)) with an effective ionic radius of more than 260 picometers have been widely investigated as A site cations that form wide-bandgap 2D/quasi-2D perovskites.⁹⁴ In these 2D/quasi-2D perovskites, the insulating bulky ammonium cations located in between layers of 3D perovskite and their bandgap can be tuned by varying the number of 3D layers by quantum confinement phenomenon.^{32,95} While this perspective is mainly focused on 3D perovskite compositions, it should be noted that instead of directly using 2D perovskites as solar absorbers, 2D perovskites can also be used to passivate 3D perovskites, which is one of the key enablers for stable and



high-performance FAPbI_3 PSCs with minimized change in bandgap,^{96–98} as will be discussed in Section 3.

2.3.2 Evolution of carrier dynamics in mixed cation perovskite. After charge generation, the performance of photovoltaic devices is governed by the competition between the recombination of charges and extraction. An efficient photovoltaic device requires a combination of high light absorption, slow charge recombination (*i.e.* long carrier lifetime), and sufficiently high charge mobility. To efficiently increase the charge carrier lifetime, an understanding of the impact of monovalent cations on the intrinsic charge carrier dynamics is essential. Although the bandgap and charge transport seem to be mainly governed by $[\text{BX}_6]^{4-}$ octahedra rather than the monovalent cations, experimental evidence shows that A-site cations significantly impact carrier lifetimes.³² It was reported that FAPbBr_3 devices exhibit a longer carrier lifetime compared to CsPbBr_3 ⁹⁹ and FAPbI_3 , as well as significantly longer lifetimes compared to MAPbI_3 , despite its inferior crystallinity and poor phase purity.^{100,101} A previous solid-state NMR study suggested a correlation between the faster reorientation dynamics of the monovalent cation and the longer charge lifetimes,¹⁰² although another study has shown that the dynamics of MA and FA are not appreciably different.¹⁰³ Computational results show that the formation of polarons on the inorganic sublattice plays a key role in stabilizing the photogenerated charge carriers, with the effect of the organic cation dynamics being negligible.^{104,105} Charge carrier dynamics in perovskites is predominantly influenced by the trap-assisted recombination, which is tightly associated with the density of the deep sub-bandgap states induced by the perovskite composition, processing method, and various other factors, which significantly hindered the investigation of the intrinsic influence of monovalent cation on the carrier dynamics.³⁶

To evaluate the impact of each monovalent cation on the charge carrier dynamics in mixed-halide perovskites, Feldmann *et al.* studied a range of very well-known mixed cation perovskite compositions with the same B-site cation (*i.e.*, Pb) and mixed X-site halide (*i.e.*, $\text{I}_{0.83}\text{Br}_{0.17}$) including single cation (SC), double cation (DC) and triple cation (TC) in $\text{MAPb}(\text{I}_{0.83}\text{Br}_{0.17})_3$, $\text{MA}_{0.2}\text{FA}_{0.8}\text{Pb}(\text{I}_{0.83}\text{Br}_{0.17})_3$ and $\text{Cs}_{0.05}\text{MA}_{0.2}\text{FA}_{0.8}\text{Pb}(\text{I}_{0.83}\text{Br}_{0.17})_3$ systems respectively.¹⁰⁶ 5% Rubidium and 10% potassium were also added as passivation agents for triple cation perovskites, denoted as Rb-TC and K-TC respectively. Transient PL spectroscopy showed a significant increase in the lifetime of PL kinetics after the incorporation of FA into MA-based films, indicating a decrease in non-radiative recombination. Similar improvement is observed for all FA-containing samples. Furthermore, the external photoluminescence quantum efficiency (PLQE) also dramatically increased from 2.7% to 22.6% after the inclusion of FA in MA perovskites (Fig. 3a), further evidencing a reduced trap-assisted recombination loss with cation mixing. The successful passivation of Cs/MA/FA perovskites with Rb or K cations is indicated by the further improvement of the external PLQE from 21.6% to 26.4% for Rb/Cs/MA/FA and 40.9% for K/Cs/MA/FA. The effect of cation mixing in reducing the non-radiative recombination losses is

also confirmed by Ledinský *et al.* They examined various perovskite compositions with temperature-dependent PL micro-spectroscopy (Fig. 3b) and the calculated Urbach energy (E_u) shows that the electronic disorder in the perovskite decreases with increasing cation multiplicity of the composition.¹⁰⁷ Indeed, the substantial improvement in PLQE and Urbach also translates to improved device performance. We have summarized the device performance of PSCs based on different perovskite compositions (SC,¹⁰⁸ DC,¹⁸ TC,³³ Rb-TC,³³ and K-TC²³) from various reports that share the same device structure (FTO/c-TiO₂/mp-TiO₂/perovskite/Spiro-OMeTAD/Au) in Fig. 3c and d. As expected from the relationship between PLQE and V_{oc} , the changes in V_{oc} of the devices closely follow the PLQE trends, showing huge improvement with cation mixing. Furthermore, a similar trend is seen for J_{sc} peaking for the TC-based perovskites, mainly caused by their enhanced carrier lifetime.¹⁸ Significantly higher values of fill factor (FF) are also achieved by Rb- and K-passivated perovskites, indicating suppression of trap-assisted recombination due to their passivation effect at the grain boundaries and interfaces. Finally, the improvement in V_{oc} , J_{sc} , and FF reflected in the average PCE of the mixed-cation perovskite devices, which reached 20.2% and 20.6% for Rb- and K-passivated TC PSCs, respectively, while achieving 10.7%, 16.4%, and 18.9% for SC, DC, and TC PSCs.

The significant improvement in optoelectronic properties of FA-containing films compared to MA single cation films can be attributed to increased crystallinity, reduction in defects in the bulk material, and suppression of ion migration, which will be discussed in a later section, due to the introduction of FA cation.^{93,106} However, it has been reported by Philippe *et al.* that a significant amount of unreacted organic cation halides was present in the FAMA perovskite films (Fig. 3e), which act as non-radiative recombination centers and exacerbated the optoelectronic performances.¹⁰⁹ The addition of Cs and Rb cations has been shown to affect the phase mixture such that the unreacted organic halides were not present anymore, as confirmed by XRD measurements from previous reports, contributing to a further reduction in trapping centers for non-radiative recombination in the films.^{18,109} It should be noted that the addition of Rb^+ alone, *i.e.*, in Rb-doped FA/MA lead iodide-bromide, has been reported to increase the trapping density and result in reduced carrier lifetime.¹¹⁰ The authors attributed it at the time to the distorting of the perovskite crystal structure, although with the current insight from ⁸⁷Rb solid-state NMR it can be attributed to the presence of the non-perovskite impurity phase RbPbI_3 .⁷⁹ On the other hand, Cs^+ incorporates into FAMA easily and results in good film quality.¹¹⁰

While both rubidium and potassium are effective additives for passivating FAMACs perovskites, they differ in how they undergo phase segregation and their subsequent effect on the optoelectronic properties.⁶³ By studying thin films of the triple cation perovskite doped with 10 mol% of Rb and K using HAADF STEM (Fig. 4), Abdi-Jalebi *et al.* reported that in the case of the K-doped film, the non-perovskite phase was finely dispersed along grain boundaries and was found to mostly contain K and Br that is validated using multivariate statistical



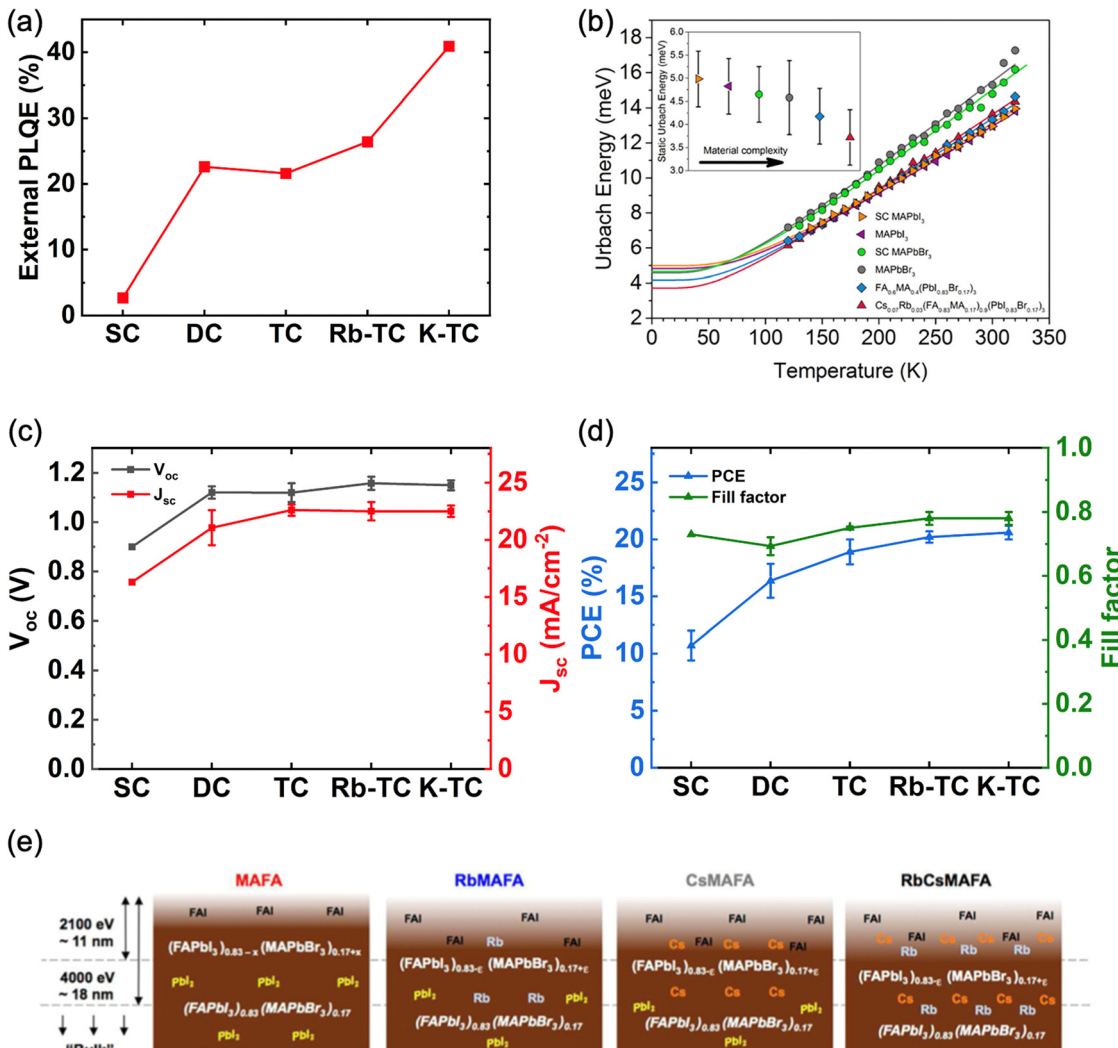


Fig. 3 (a) External PLQE of perovskite thin films with a variety of compositions. Films were ~ 550 nm thick on glass substrates, measured at an excitation density of 1015 cm^{-2} (approximately solar illumination conditions). Figure plotted based on data from ref. 106. (b) Temperature dependence of Urbach energy (E_u) for perovskite thin films with various compositions. The inset shows the static part of E_u . Adapted with permission from ref. 107. Copyright © 2020, American Chemical Society. (c) V_{oc} , J_{sc} and (d) PCE and fill factor of perovskite solar cells based on $\text{MAPb}(\text{I}_{0.83}\text{Br}_{0.17})_3$ ¹⁰⁸ (SC), $\text{MA}_{0.17}\text{FA}_{0.83-}\text{Pb}(\text{I}_{0.83}\text{Br}_{0.17})_3$ ¹⁸ (DC), $\text{Cs}_{0.05}\text{MA}_{0.17}\text{FA}_{0.83}\text{Pb}(\text{I}_{0.83}\text{Br}_{0.17})_3$ ³³ (TC), $\text{Rb}_{0.05}(\text{Cs}_{0.05}\text{MA}_{0.17}\text{FA}_{0.83})_{0.9}\text{Pb}(\text{I}_{0.83}\text{Br}_{0.17})_3$ ³³ (Rb-TC) and $\text{K}_{0.1}(\text{Cs}_{0.05}\text{MA}_{0.17}\text{FA}_{0.83})_{0.9}\text{Pb}(\text{I}_{0.83}\text{Br}_{0.17})_3$ ²³ (K-TC) reported in different literature. All PSCs are fabricated in $\text{FTO}/\text{c-TiO}_2/\text{mp-TiO}_2/\text{perovskite}/\text{Spiro-OMeTAD}/\text{Au}$ structure with no other modifications. Error bars are included in all data points except for SC PSCs, where only error bars for PCEs were shown in the original report. (e) Schematic illustration of the chemical distribution of perovskite materials with multiple cation systems based on HAXPES (Hard X-ray Photoelectron Spectroscopy). Adapted with permission from ref. 109. Copyright © 2017, American Chemical Society.

analyses with the combination of scanning transmission electron microscopy (STEM) and energy-dispersive X-ray spectroscopy (EDS).^{63,111} On the other hand, the Rb-doped film exhibited large, micron-sized grains of a rubidium-rich phase with no evidence of grain boundary passivation. The rubidium-rich phase has been previously identified to be a mixed-halide rubidium haloplumbate.^{61,62} The differences in microstructure, as probed by STEM, observed for the two types of films are strongly correlated with the corresponding PLQE results: K doping increased it from 18% to as much as 52% (for 20 mol% K) while Rb doping yielded $\sim 24\%$ (for 5 mol% Rb), with no further increase at higher Rb loading ratios. Since PLQE is related to the concentration of surface trap states, with fewer trap states leading to higher

PLQE,¹¹² the pronounced increase in PLQE for the K-doped material is consistent with K passivation of the surface defects present at grain boundaries.²³ The authors proposed that the morphological differences of the K- and Rb-rich phases as well as the different optimal doping levels can be explained by differences in solubility of the doping precursors (KI and RbI) in the precursor solution, leading to differences in crystallization dynamics during the film formation.

2.3.3 Inhibition of ion migration in mixed halide perovskites. Unlike conventional inorganic solar cell materials, the charged ions of perovskite are mobile under light illumination, electric field, or elevated temperature. The migration of ions creates vacancies or other defects in the crystal structure and

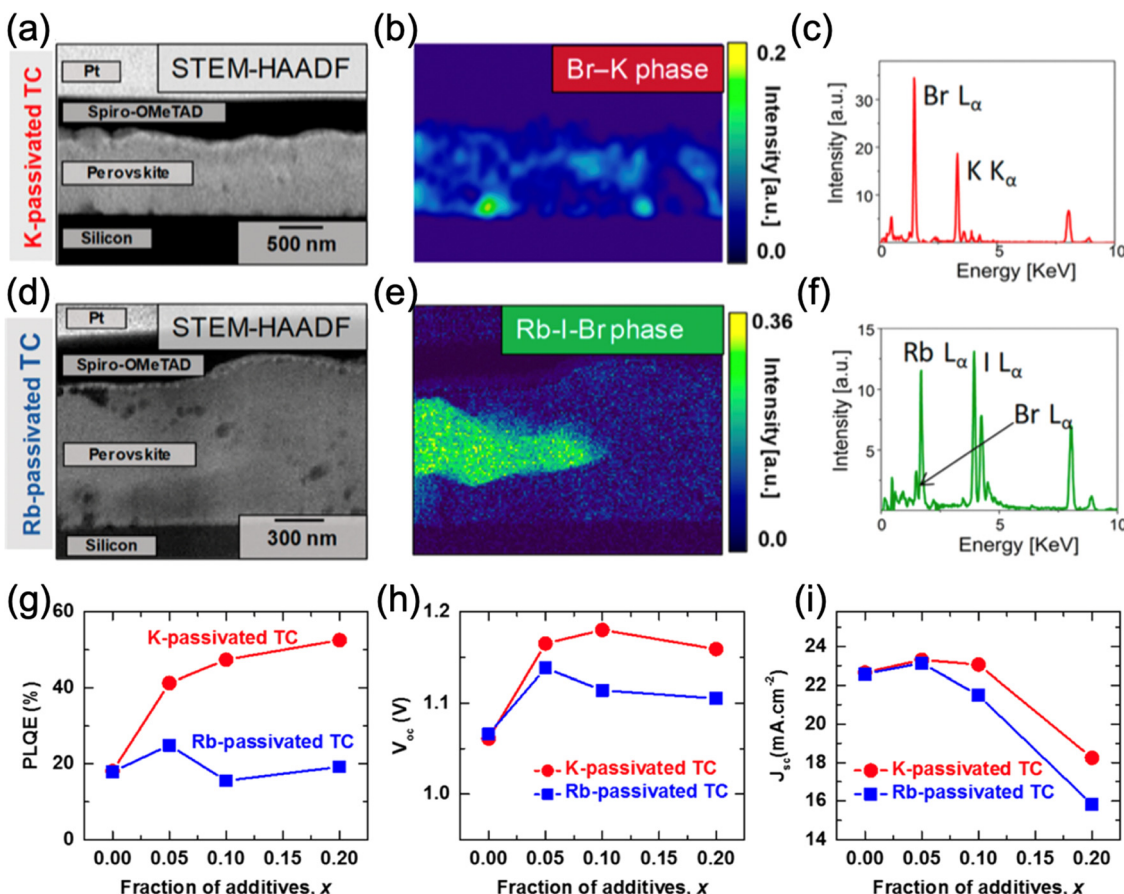


Fig. 4 (a) HAADF STEM image of a cross-section triple-cation (TC) perovskite thin film with 10% K content. (b) Non-negative Matrix Factorization (NMF) showing the KBr phase and (c) the EDX spectra. (d) HAADF STEM image of the cross-section TC perovskite thin film with 10% Rb content. (e) NMF showing the Rb-I-Br phase and (f) the EDX spectra. (g) PLQE, (h) V_{oc} and (i) J_{sc} of the K- and Rb-passivated TC perovskites as a function of K and Rb content. Adapted with permission from ref. 63. Copyright © 2018, American Chemical Society.

provides a pathway for phase segregation, current–voltage hysteresis, and the degradation of PSCs during operation. Fig. 5a shows the possible migration pathways in perovskite thin films. How easily an ion species migrates in the bulk material is evaluated by its migration rate (r_m), which is determined by the activation energy (E_a) and the relationship $r_m \propto e^{E_a/k_B T}$, where k_B and T are the Boltzmann constant and temperature, respectively. The smaller the E_a , the more easily the ion migrates in the bulk. Based on this, two general strategies are implemented to mitigate the ion migration phenomenon: (1) increasing the activation energy for ion migration and (2) reducing the density of mobile ions in the perovskite film ref. 32.

The formation energy of anion and cation vacancies and the activation energy for ion migration are strongly related to the Coulomb interaction between ions within the crystal lattice. Therefore, one of the main methods to suppress ion migration is by mixing cations of different sizes. The local distortion in crystal lattice results in a larger energy required for ions to migrate within the lattice and subsequently inhibits ion migration, improving the thermo- and photostability of the devices. For example, Tan *et al.* performed a temperature-dependent

conductivity measurement on FAPbI_3 , $\text{MA}_{0.05}\text{FA}_{0.95}\text{PbI}_3$, and $\text{Cs}_{0.05}\text{FA}_{0.95}\text{PbI}_3$ lateral devices to obtain the ion migration activation energy.¹¹³ They observed that E_a increases with the increasing mismatch in A-site cation sizes (Fig. 5b–d), with both mixed cation perovskites showing an increased energy barrier for ion migration compared to FAPbI_3 . However, excess lattice strain can induce new defects in the lattice to relieve the residual strain, creating new pathways for ion migration and detrimentally reducing the activation energy.²⁸ Therefore, finding an optimal amount of cation substitution is important for ion migration using mixed cations. Furthermore, Mosconi *et al.* reported that the MA cations can promote ion migration by reorienting their charge distribution according to the ion movement.¹¹⁴ Mixing MA⁺ with less polar cations that exhibit lower orientational mobility such as FA⁺ and Cs⁺, combined with the tuning of local distortion within the lattice, effectively suppresses ion migration and improves device operational stability, as evidenced by various reports.^{115,116}

Apart from point defects such as cation and anion vacancies, the existence of grain boundaries is also a major pathway for ion migration. The addition of alkali cations such as Rb⁺ and K⁺ is also widely used to reduce ion migration by partial blockage

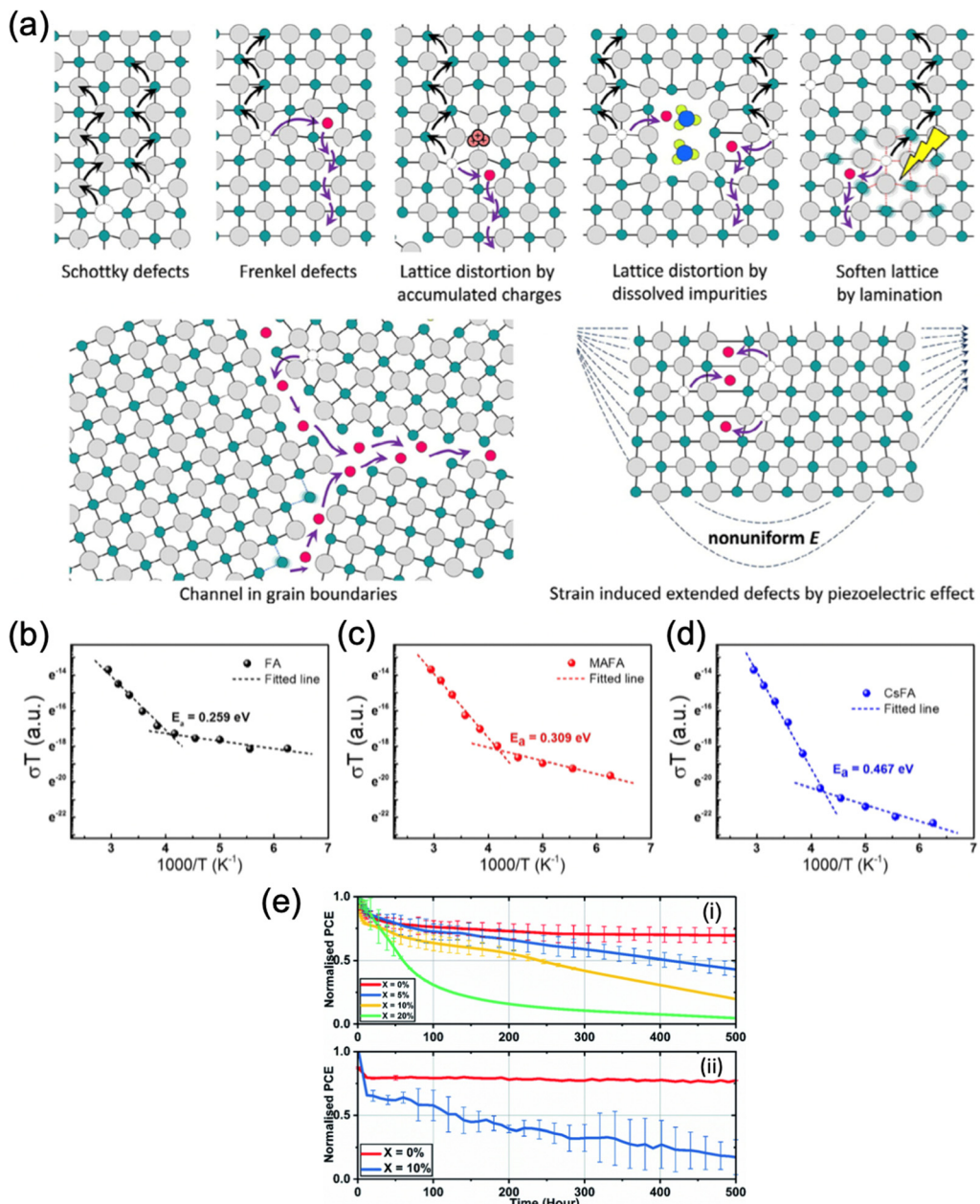


Fig. 5 Inhibition of ion migration using multiple cations. (a) Schematic diagram of ion migration pathways in perovskite thin films. Adapted with permission from ref. 117. Copyright © 2016, American Chemical Society. (b)–(d) Temperature-dependent conductivity and the calculated activation energy for ion migration of the (b) FAPbI₃, (c) MA_{0.05}FA_{0.95}PbI₃ and (d) Cs_{0.05}FA_{0.95}PbI₃ lateral devices. Adapted with permission from ref. 118. Copyright © 2020, WILEY-VCH Verlag GmbH & Co. KGaA, Weinheim. (e) Long-term device stability of TC perovskites based on (i) SnO₂ and (ii) TiO₂ with varying level of doped KI.¹¹⁹ Adapted with permission from ref. 119. Copyright © 2020, The Royal Society of Chemistry.

of ion migration pathways and defect passivation. Son *et al.* demonstrated that the addition of a small amount of Na⁺, K⁺ or Rb⁺ suppressed the hysteresis of PSCs based on MAPbI₃, FAPbI₃, FA_{0.85}MA_{0.15}PbI_{2.55}Br_{0.45} and FA_{0.85}MA_{0.1}Cs_{0.05}PbI_{2.7}Br_{0.3} to different extents.¹²⁰ In particular, adding an optimal concentration of KI completely eliminated the hysteresis effect. Theoretical studies indicate that these undersized alkali additives increase the formation energy of interstitial defects and subsequently suppress the ion migration.¹²¹ Abdi-Jalebi *et al.* also demonstrated significant mitigation of ion migration with

potassium passivation.²³ However, they attributed the effect to the excess iodide that reduces the halide vacancies and K⁺ immobilized the halide ions by forming benign, potassium-rich compounds at the grain boundaries and surfaces. However, both Rb- and K-doped perovskites exhibit considerable instability under humid conditions. While both types of cells exhibit relatively good stability under dry nitrogen (a drop to 95% after 500 hours and ~80% after 300 hours for Rb and K doping, respectively),^{23,24} reports have shown that Rb-doped perovskite thin films have been found to be particularly unstable,

compared to their undoped counterparts.⁶² Hu *et al.* reported a ~70% drop in PCE for Rb- and Rb/Cs-doped perovskite devices after 1 day of 75% RH exposure, while the undoped reference films of MA/FA and Cs/MA/FA have only lost ~25% of the initial PCE during the same period. This result was rationalized by the rapid formation of the Rb-rich RbPb₂I₄Br non-perovskite phase, as evidenced by EDX mapping. K-doped perovskite thin films showed relatively better humidity stability compared to Rb-doped thin films, as evidenced by the fact that the exposure to 30% relative humidity (RH) for 1 week in the dark leads to the formation of needle-like crystals in the Rb-doped thin film, while no changes are apparent in the K-doped material.⁶³ However, under higher humidity (~50%), undesired non-perovskite KBr phase segregated on the film surface. Indeed, Alanazi *et al.* reported that perovskites passivated by 5% or 10% KI in the initial precursor suffer from phase instability under 35–45% relative humidity and at a temperature of 42 ± 3 °C over 500 hours of illumination, resulting in a worse performance compared to the undoped devices, whereas devices doped with 20% KI experienced rapid, critical failure due to the formation of KBr (Fig. 5e).

3. Towards simpler perovskite compositions

Composition engineering by mixing FA⁺ with MA⁺, Cs⁺, Rb⁺, K⁺, and the addition of Br⁻ have been demonstrated to be effective strategies to improve the optoelectronic properties and stability of FA-based perovskites by improving their carrier dynamics, ion migration, crystallinity, and the overall stability, as discussed in the above section. Nevertheless, mixed-cation halide perovskite still faces the challenge of phase stability, such as light-induced halide segregation. More importantly, the substitution of FA⁺ inevitably increases the bandgap and sacrifices the light absorption in the near-infrared region. Therefore, to preserve the preferred bandgap of FAPbI₃, more subtle phase stabilization strategies other than composition engineering have been researched extensively in recent years.

One of the most widely used methods to stabilize phase-pure α -FAPbI₃ is using chloride-based additives (e.g. formamidinium chloride (FACl) and methylammonium chloride (MACl)) in precursor solution for intermediate phase engineering.¹²² During fabrication, MACl first induces the formation of intermediate mixtures to the pure α -FAPbI₃ phase at room temperature while suppressing the growth of the δ -FAPbI₃ phase (Fig. 6a). Upon further annealing, MACl decomposes into MA⁺ and FACl, which can readily evaporate with annealing, while the intermediate mixtures are converted into highly crystalline α -FAPbI₃ phase with only small traces of residual MA⁺ (~5 mol%) even with a high initial MACl concentration (~40 mol%) in the precursor solution. The resulting films only exhibit a minor blueshift of the bandgap (~1.50 to 1.53 eV), which leads to a PCE of 24.02% (certified 23.5%) for PSCs based on this method (Fig. 6b and c). Similarly, FACl as an intermediate additive was reported by Mu *et al.* and a PCE of over

20% was achieved.¹²³ Seok *et al.* also reported that adding isopropylammonium chloride (iPAmHCl) together with MACl to the precursor solution could further stabilize the α -FAPbI₃ phase.¹²⁴ After thermal annealing, the remaining iPAmHCl passivated the grain boundaries of FAPbI₃ and reduced the defects, which resulted in a certified PCE of 23.9%. Furthermore, formamidinium formate (FAFa) was introduced recently as a co-additive with MACl in order to produce highly stable α -FAPbI₃ perovskite films.⁵ The close interaction of the pseudo-halide formate (HCOO⁻) anions with the Pb²⁺ and FA cations causes a plummet in iodide vacancies at the grain boundaries. The resulting perovskite film with enhanced crystallinity led to 450 hours of operational stability and a certified substantial PCE of 25.2%.

Surface energy manipulation is another promising strategy to stabilise α -FAPbI₃.^{26,31} Lu *et al.* recently demonstrated the use of methylammonium thiocyanate (MASCN) vapor treatment to convert the non-photoactive δ -FAPbI₃ to the α phase at 100 °C, significantly under the thermodynamic phase-transition temperature.²⁶ By surrounding a spin-coated yellow δ -FAPbI₃ film in a MASN vapor environment for ~5 min, pure α -FAPbI₃ film was formed, as evidenced by minimal change in bandgap energy and XRD results compared to the reference pure FAPbI₃. By performing solid-state NMR and molecular dynamics simulations, they confirmed that MASN was not incorporated into the perovskite lattice. Instead, SCN-ions displace the iodides and bond with Pb²⁺ ions on the surface of δ -FAPbI₃. This process disrupts the top surface of face-sharing octahedra and encouraged the formation and stabilization of corner-sharing Pb-I-SCN structures of α -FAPbI₃, which in turn triggers the full conversion to α -FAPbI₃ below the thermodynamic phase-transition temperature. Once the phase-pure α -FAPbI₃ was formed, it remained kinetically stable in its photoactive phase even after 500 hours of annealing at 85 °C and PSC devices with >23% and long-term stability were achieved. Very recently, Doherty *et al.* showed that the black perovskite phase of FAPbI₃ can be stabilized without the use of MA-containing additives.³¹ The authors used 5 mol% EDTA added to the precursor solution of FAI and PbI₂ and found that thin films made using this composition lead to materials stable in ambient air for at least 1000 hours, under 1 sun illumination for at least 100 hours and resistant to heating at 100 °C in ambient air for at least 24 hours. This exceptional stability has been attributed to two factors: (a) EDTA binding to the perovskite surface elucidated by solid-state NMR and NQR (Nuclear Quadrupole Resonance), and (b) slight crystal symmetry modification induced by the EDTA molecules, during the crystallite growth phase (templating effect). This symmetry modification consists of the introduction of a small octahedral tilt which prevents the transition to the hexagonal δ polymorph of FAPbI₃. Notably, it does not compromise the optical properties of the resulting material, which makes it highly promising for PSCs.

For solution-processed perovskites, the solvents used for dissolving the perovskite precursors play a key role in the crystallization of perovskites. Lewis base additives as solvents



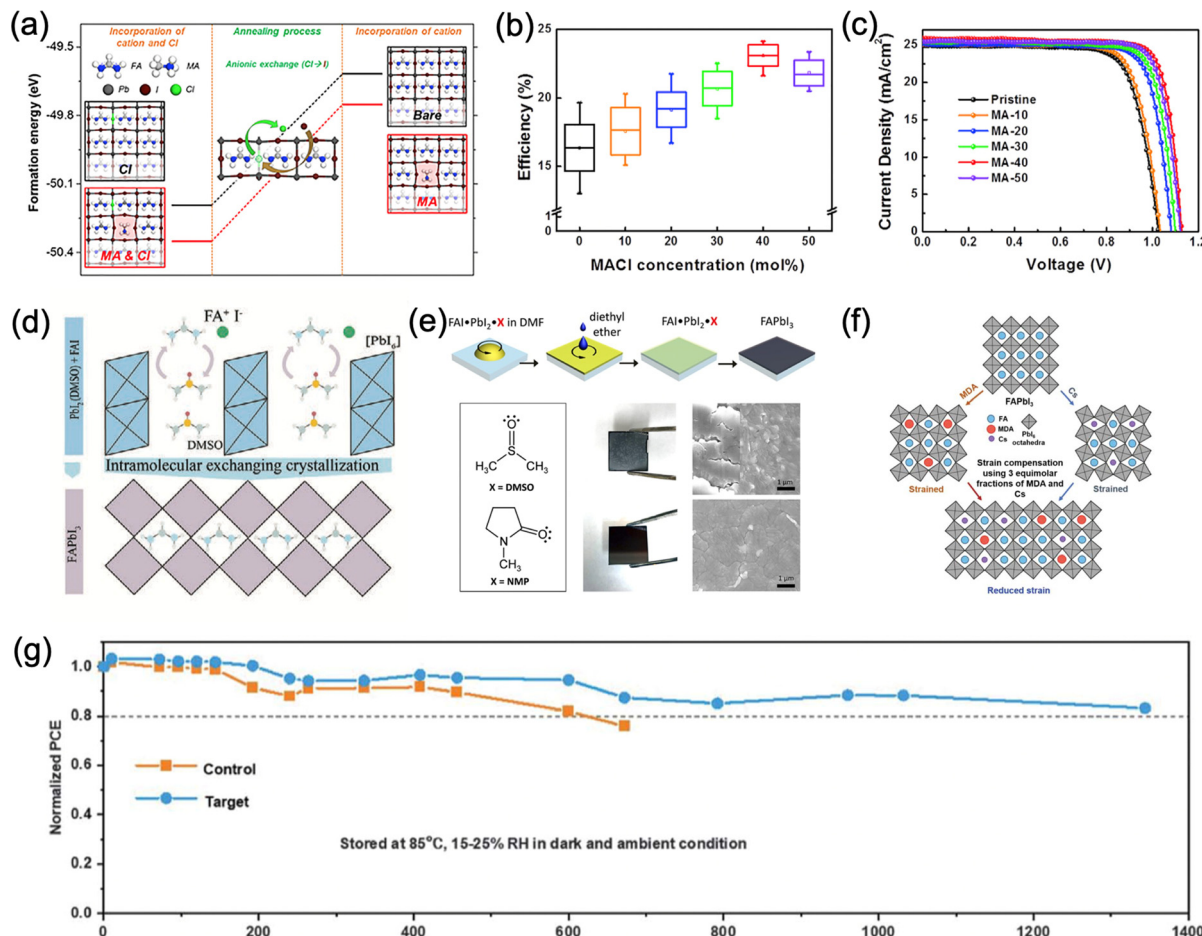


Fig. 6 (a) Theoretical calculations of the crystal structure and the formation energy of FAPbI₃ and the ones prepared with Cl, MA, or MACl.¹²² (b) Efficiency distribution and (c) J–V curves of FAPbI₃ devices prepared with various amounts of MACl.¹²² Panel (a)–(c) adapted with permission from ref. 122. Copyright © 2019, Elsevier Inc. (d) Schematic diagram of the FAPbI₃ crystallization process with the assistance of DMSO Lewis base. DMSO molecules are intercalated in PbI₂ and exchange with FAI.¹⁰⁵ Adapted with permission from ref. 125. Copyright © 2019, The American Association for the Advancement of Science. (e) Schematic illustration of the fabrication process using DMSO as a Lewis base and the effect of DMSO and NMP on the morphology of perovskite thin films.¹²⁶ Adapted with permission from ref. 105. Copyright © 2018, American Chemical Society. (f) Schematic diagram of strain relaxation of α -FAPbI₃ after incorporation of MDA⁺ and Cs.²⁸ (g) Comparison of thermal stability between MDA/Cs incorporated PSC with the reference FAPbI₃ PSC.²⁸ Panel (f) and (g) are adapted with permission from ref. 28. Copyright © 2019, The American Association for the Advancement of Science.

offer a way to control the intermediate phase to stabilize phase-pure α -FAPbI₃. The introduction of Lewis bases with lone-pair electrons from O-donors, S-donors, or N-donors forms intermediate complexes with the undercoordinated Pb²⁺ in the perovskite precursor solution and has been suggested to mediate the crystallization process to form high-quality α -FAPbI₃ films.^{125,126} In 2015, Seok *et al.* used the Lewis acid-base adduct FAI-PbI₂-DMSO by introducing DMSO into the PbI₂ layer during a two-step sequential deposition to form α -FAPbI₃ films with large grains and efficiencies exceeding 20%¹²⁵ (Fig. 6d). Later, Lee *et al.* demonstrated a more stable perovskite intermediate FAI-PbI₂-NMP that produced high-performance α -FAPbI₃ devices with high reproducibility (Fig. 6e). Although DMSO was replaced with NMP, the phase purity was still not guaranteed, and Cs⁺ ions were required to improve it.¹²⁶ They also concluded that an effective Lewis base to stabilize the intermediate should have (1) hydrogen bond accepting ability,

(2) a sterically accessible electron donating group, and (3) matching hardness between the Lewis acid and base. Other Lewis bases such as thiourea as the S-donor Lewis base,¹²⁷ and $-\text{NH}_2$ phenylalkylamines have also been used to control the perovskite intermediates.¹²⁸ Later, Salim *et al.* interestingly demonstrated that the use of NMP also enables ambient fabrication of FAPbI₃ PSCs (RH 40–60%) with drastically improved long-term stability ($T_{80} = 112$ days, unencapsulated) and slightly improved PCE (15.53%) compared to reference devices fabricated under nitrogen ($T_{80} = 21$ days, 14.36%),¹²⁹ despite multiple reports evidencing accelerated α to δ phase transition of FAPbI₃ triggered by the presence of moisture.^{130,131} By comparing FAPbI₃ samples fabricated under ambient air or N₂ with Raman spectroscopy and XPS, the formation of Pb–O bonds was observed for FAPbI₃ (air) samples during aging whereas FAPbI₃ (N₂) samples directly transformed into the δ -phase. They suggested that PbO_x species form

intrinsically under ambient conditions with the use of NMP additive and the presence of Pb–O bonds blocks the expansion of the δ -phase, stabilizing the black α -phase. Moreover, the addition of PbS quantum dots (QDs) under ambient conditions further improved the T_{80} to 145 days with device efficiency reaching 17.1%. Further addition of MACl boosted the champion device efficiency to 19.4%. The potential of ambient fabrication of FAPbI₃ devices with great efficiency and stability paves the way to future industrialization of such devices, though the detailed mechanism of such stability improvement, especially the role of NMP and water during the process, still needs further investigation.

The incorporation of layered two dimensional (2D) perovskites is another available option to stabilize black FAPbI₃. Although these 2D perovskites on their own possess exceptional stability, their efficiency is still lagging behind their 3D counterparts, mainly due to the limited out-of-plane charge transport ability caused by the bulky organic cations.⁴⁷ However, when the layered perovskites are used as capping layers on top of 3D perovskites or inserted into the grain boundaries of 3D perovskites (Fig. 7a and b), they can stabilize the cubic FAPbI₃ phase with excellent device performance and stability. For example, Liu *et al.* introduced a 2D IBA₂FAPb₂I₇ as a capping layer by spin-coating an IPA solution of isobutylammonium iodide (IBAI) on top of the FAPbI₃ perovskite layer.⁹⁶ The presence of a stable layered perovskite significantly reduced the trap density and promoted the formation of high-quality FAPbI₃ films. In addition, the hydrophobicity of IBA⁺ can greatly improve the moisture stability of the perovskite. The resulting 2D/3D perovskite devices achieved an efficiency of 22.7% and maintained around 85% of their initial efficiency after 500 hours at 80 °C under full-sun illumination. Apart from IBA⁺, phenylethylammonium (PEA⁺) is also a common cation to stabilize FAPbI₃.^{97,98} When PEA⁺ cations are introduced into

the precursor solution, they promote the formation of high crystallinity FAPbI₃ and form 2D PEA₂PbI₄ perovskites at the grain boundaries, which substantially enhances the moisture stability (Fig. 7c) and inhibits ion migration through grain boundaries. Moreover, the relatively low charge transport ability of 2D perovskite facilitates longitudinal charge transport and reduces the non-radiative recombination at the grain boundaries. Lee *et al.* reported that the incorporation of 1.67 mol% of PEA₂PbI₄ resulted in the formation of phase-pure FAPbI₃ with the bandgap energy being unchanged (1.48 eV) and improved carrier lifetime.⁹⁷ PSC devices based on this 2D/3D perovskite exhibited a stabilized PCE of 20.64% and significantly improved the operation stability (Fig. 7d). Another example of such 2D perovskite as the capping layer is pentafluorophenylethylammonium (FEA) lead iodide $[(\text{FEA})_2\text{PbI}_4]$,¹³² where the perfluorinated benzene ring in the molecule provides ultrahydrophobicity compared to PEA⁺ based perovskite. Apart from mitigating the exposure of 3D perovskite to moisture, the perfluorinated benzene ring also promotes hole extraction and inhibits interlayer ion migration. The device efficiency was improved to 22.2% for 3D/2D PSCs compared to 20.0 for the 3D reference and an impressive J_{sc} of 25.8 mA cm⁻² was achieved. The 3D/2D PSC retained 90% of its initial efficiency after 1000 hours under 1 sun irradiation at RH 40% while its 3D counterpart dropped to 43%.

The use of FAPbI₃ powder as a precursor instead of the commonly used solution mixture of FAI and PbI₂ is a promising method to achieve high-performance FAPbI₃ PSCs with excellent stability. The direct dissolution of FAPbI₃ avoids the problem of nonstoichiometric perovskites and high defect density that are detrimental to the stability, performance, and reproducibility of the PSC devices.^{133,134} The α -FAPbI₃ single crystal powders are prepared using the inverse temperature crystallization method where the solvents and anti-solvents of

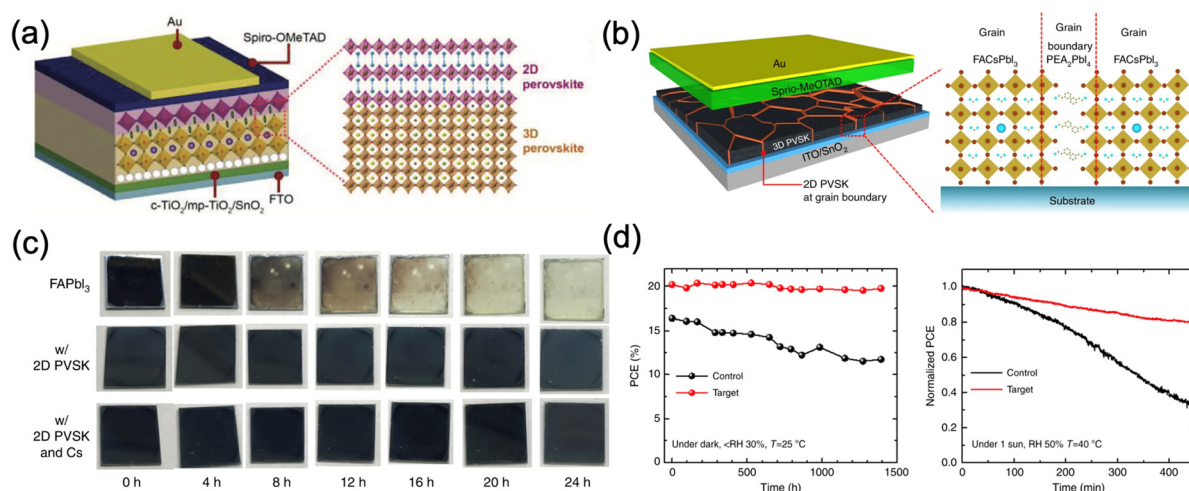


Fig. 7 (a) and (b) Schematic diagrams of the PSC devices with 2D perovskite as (a) a capping layer and (b) grain boundary passivator.⁹⁷ (c) Moisture stability of FAPbI₃, FAPbI₃ with PEA⁺, FAPbI₃ with PEA⁺ and Cs⁺ under 80 ± 5% relative humidity (RH).⁹⁷ (d) Stability of FAPbI₃ with 1.67 mol% of PEA₂PbI₄ in the dark with controlled humidity and maximum point tracking (MPP) of the devices under ambient conditions under 1 sun without encapsulation.⁹⁷ Panels (b)–(d) are adapted with permission from ref. 97. Copyright © 2018, Jin-Wook Lee *et al.*



perovskite precursors are carefully chosen based on their solubilities in different temperatures, and α -FAPbI₃ single crystal powders are directly formed during the controlled cooling-induced crystallization.¹³⁵ Most importantly, the use of single crystal powders can be combined with composition engineering, intermediate phase engineering, and other approaches, which have been the main driving forces for α -FAPbI₃ based PSCs to reach efficiencies beyond 25%.^{5,39} Another straightforward way for preparing halide perovskite powders is by means of mechano-synthesis, and PSCs made using this strategy have also been gaining prominence, although it has not yet been applied to α -FAPbI₃.^{136,137}

Apart from the strategies mentioned above, other phase stabilization strategies, such as the addition of hydrohalic acid (HI,¹³⁸ HCl¹³⁹) and temperature regulation during crystallisation,^{140,141} all showed great potential for stabilizing α -FAPbI₃ and led to device performances on par or beyond that of multiple cation/anion perovskites.

4. Conclusion and outlook

Fabricating highly efficient PSCs with long-term stability has been the ultimate goal in the field of perovskite photovoltaics. As a result of its optimal bandgap of 1.47 eV, FAPbI₃ is currently one of the most promising perovskites for high-efficiency solar cells. However, under ambient conditions, its black phase is less stable. Composition engineering by cation and halide mixing enables the long-term stabilization of FA dominant perovskites under operational conditions through entropic stabilization, reduction in non-radiative defect states, and increased carrier lifetime. Further passivation through the addition of a small amount of alkali monovalent cations such as Rb and K also significantly improves the optoelectronic properties of the perovskite and leads to more efficient solar cells. So far, triple-cation (Cs/FA/MA) perovskites with dominant FA and a small content of MA and Cs have been able to give highly reproducible efficiencies above 22%. Furthermore, Miyasaka *et al.* demonstrated that highly reproducible and high-quality triple-cation perovskite solar cells can be fabricated even in ambient air (<RH 25%), achieving PCEs of over 20% with long-term stability of up to 18 weeks,¹⁹ which is essential for the future development of cost-effective manufacture since it allows the elimination of an expensive inert atmosphere that is usually required for PSC fabrication. However, the replacement of FA⁺ with smaller cations such as MA⁺ and Cs⁺ induces an inevitable increase in the bandgap energy and loss of photocurrent in the near-infrared region, limiting its potential for more efficient solar cells. Furthermore, the inclusion of additional cations adds exceptional complexity to the phase composition of the resulting solid material. Solid-state NMR has been essential in unraveling this complexity. With its wide range of isotope-dependent experimental strategies, it provided unparalleled information on the fate of Cs⁺, Rb⁺, and K⁺ in multicomponent halide perovskite compositions, evidencing various phase segregation phenomena that are directly

responsible for the observed modulation of optoelectronic properties. This complexity is also reflected in the optimization of the perovskite composition, which becomes a multidimensional problem. This is illustrated well by the observation that the amount of unreacted organic species in halide perovskite thin films increases with the increasing number of cations used.¹⁰⁹ The addition of multiple cations also introduces extra sources of instability in the system. Apart from MA⁺ which is known for its volatile nature, both K- and Rb-passivated perovskite devices show significant susceptibility to moisture degradation, limiting the device performance under ambient conditions.⁶³ Since any variation in the A-site cation composition will impact the phase transition, crystallization, and optoelectronic properties of the system, finding the suitable composition of the perovskite experimentally is an energy-intensive task. A more in-depth understanding of the role of the monovalent cations in these aspects is critical to further boosting the performance and stability of multiple cation/anion PSCs. Considering the complexity of multiple cation/anion perovskite systems, the use of computational chemistry and machine learning is expected to be crucial for finding new, improved compositions using the cation mixing approach.

More recently, investigating alternative ways to stabilize phase-pure α -FAPbI₃ that retains its desired bandgap has been the focus of the research field. Various strategies have been successfully developed to achieve the stabilized black phase, including additive engineering, dimensionality engineering, temperature regulation during crystallization, and the use of FAPbI₃ single crystal powder, pushing the efficiency of PSCs based on FAPbI₃ above 25%, exceeding those of multiple cation/anion perovskites. However, most of these stabilization strategies only realize a metastable photoactive phase which eventually converts back to the equilibrium hexagonal non-perovskite phase.³² Interestingly, surface energy manipulation has been recently discovered to be a promising approach to stabilize the black perovskite phase of FAPbI₃ by using SCN⁻ or EDTA to template the crystal growth of perovskites to favor the formation of α -FAPbI₃.^{26,142} More understanding of the factors that impact the thermodynamic stability of α -FAPbI₃ is required to identify the exact origin of this stabilization effect and whether this is a manifestation of a more general phenomenon, or perhaps just one of many possibilities to stabilize the black FAPbI₃ without the need for cation mixing. One other problem for FAPbI₃ based PSCs is that the widely used MACl as a stabilizer inevitably introduces the unstable MA⁺ into the system in addition to slightly blue shifting the bandgap. Alternative stabilizers that are less prone to degradation and do not affect the bandgap need to be developed.

Due to the rapid development of PSCs in terms of both PCE and long-term stability, industrialization of the technology has attracted enormous interest in the field. Ambient fabrication of solar cell modules is one of the key factors to produce cost-effective FA based PSCs. Since the α - to δ -phase transition is accelerated in the presence of moisture and oxygen, ambient fabrication of FAPbI₃ is extremely challenging compared to the mixed-cation approach,^{130,131} though fabrication of high-efficiency



PSCs with controlled humidity (RH < 20%) has been reported by several works^{5,9} and the use of NMP as an additive for PSC fabrication under moderate/high RH of 40–60% looks promising for the future development of ambient fabrication of PSCs in an industrial setting. However, mechanistic investigations as well as in-situ structural analysis on the formation and degradation of FAPbI₃ perovskite are required to truly understand the role of these additives on the perovskite stability and improve the reproducibility of devices. In addition, although large-scale preparation of PSCs with methods such as blade coating,¹⁴³ screen printing,¹⁴⁴ slot-die coating¹⁴⁵ and inkjet printing¹⁴⁶ have been developed for other PSCs, their compatibility with phase-pure FAPbI₃-based PSCs still requires improvement.

Ultimately, we believe that with appropriate, stable passivating agents and fundamental understanding of the perovskite materials, phase-pure FAPbI₃ is a highly promising candidate for the next generation of PSCs approaching the theoretical limit.

Conflicts of interest

There are no conflicts to declare.

Acknowledgements

Q. L. is grateful for the support from the Chinese Scholarship Council (CSC) and the Faculty of Mathematical & Physical Sciences (MAPS) at University College London (UCL). M. A.-J. acknowledges the Royal Society (RGS\R1\211068), Cambridge Materials Limited, and Wolfson College, University of Cambridge for their funding and technical support. The authors acknowledge the ACT programme (Accelerating CCS Technologies, Horizon2020 Project No. 691712) and Department for Business, Energy and Industrial Strategy for the financial support of the NEXTCCUS project (project ID: 327327). We acknowledge UCL Research, Innovation & Global Engagement, Cornell-UCL Global Strategic Collaboration Awards team for their financial Support. D. J. K. acknowledges support from the University of Warwick.

References

- 1 S. D. Stranks and H. J. Snaith, *Nat. Nanotechnol.*, 2015, **10**, 391–402.
- 2 J. Yoon, H. Sung, G. Lee, W. Cho, N. Ahn, H. S. Jung and M. Choi, *Energy Environ. Sci.*, 2017, **10**, 337–345.
- 3 NREL Best Research-Cell Efficiency Chart, <https://www.nrel.gov/pv/cell-efficiency.html>, accessed 31 July 2022.
- 4 M. Kim, J. Jeong, H. Lu, T. K. Lee, F. T. Eickemeyer, Y. Liu, I. W. Choi, S. J. Choi, Y. Jo, H. B. Kim, S. I. Mo, Y. K. Kim, H. Lee, N. G. An, S. Cho, W. R. Tress, S. M. Zakeeruddin, A. Hagfeldt, J. Y. Kim, M. Grätzel and D. S. Kim, *Science*, 2022, **375**, 302–306.
- 5 J. Jeong, M. Kim, J. Seo, H. Lu, P. Ahlawat, A. Mishra, Y. Yang, M. A. Hope, F. T. Eickemeyer, M. Kim, Y. J. Yoon, I. W. Choi, B. P. Darwich, S. J. Choi, Y. Jo, J. H. Lee, B. Walker, S. M. Zakeeruddin, L. Emsley, U. Rothlisberger, A. Hagfeldt, D. S. Kim, M. Grätzel and J. Y. Kim, *Nature*, 2021, **592**, 381–385.
- 6 Y. H. Kim, S. Kim, A. Kakekhani, J. Park, J. Park, Y. H. Lee, H. Xu, S. Nagane, R. B. Wexler, D. H. Kim, S. H. Jo, L. Martínez-Sarti, P. Tan, A. Sadhanala, G. S. Park, Y. W. Kim, B. Hu, H. J. Bolink, S. Yoo, R. H. Friend, A. M. Rappe and T. W. Lee, *Nat. Photonics*, 2021, **15**(2), 148–155.
- 7 H. J. Snaith, *Nat. Mater.*, 2018, **17**, 372–376.
- 8 N. J. Jeon, J. H. Noh, W. S. Yang, Y. C. Kim, S. Ryu, J. Seo and S. Il Seok, *Nature*, 2015, **517**, 476–480.
- 9 Q. Jiang, Y. Zhao, X. Zhang, X. Yang, Y. Chen, Z. Chu, Q. Ye, X. Li, Z. Yin and J. You, *Nat. Photonics*, 2019, **13**(7), 460–466.
- 10 M. Abdi-Jalebi, M. I. Dar, S. P. Senanayak, A. Sadhanala, Z. Andaji-Garmaroudi, L. M. Pazos-Outón, J. M. Richter, A. J. Pearson, H. Sirringhaus, M. Grätzel and R. H. Friend, *Sci. Adv.*, 2019, **5**, 2.
- 11 A. Kojima, K. Teshima, Y. Shirai and T. Miyasaka, *J. Am. Chem. Soc.*, 2009, **131**, 6050–6051.
- 12 S. P. Senanayak, B. Yang, T. H. Thomas, N. Giesbrecht, W. Huang, E. Gann, B. Nair, K. Goedel, S. Guha, X. Moya, C. R. McNeill, P. Docampo, A. Sadhanala, R. H. Friend and H. Sirringhaus, *Sci. Adv.*, 2017, **3**, e1601935.
- 13 N. Pellet, P. Gao, G. Gregori, T. Y. Yang, M. K. Nazeeruddin, J. Maier and M. Grätzel, *Angew. Chem., Int. Ed.*, 2014, **53**, 3151–3157.
- 14 K. Wang, Z. Jin, L. Liang, H. Bian, D. Bai, H. Wang, J. Zhang, Q. Wang and L. Shengzhong, *Nat. Commun.*, 2018, **9**(1), 1–8.
- 15 H.-S. Kim, A. Hagfeldt and N.-G. Park, *Chem. Commun.*, 2019, **55**, 1192–1200.
- 16 A. A. Zhumekenov, M. I. Saidaminov, M. A. Haque, E. Alarousu, S. P. Sarmah, B. Murali, I. Dursun, X. H. Miao, A. L. Abdelhady, T. Wu, O. F. Mohammed and O. M. Bakr, *ACS Energy Lett.*, 2016, **1**, 32–37.
- 17 M. T. Weller, O. J. Weber, J. M. Frost and A. Walsh, *J. Phys. Chem. Lett.*, 2015, **6**, 3209–3212.
- 18 M. Saliba, T. Matsui, J. Y. Seo, K. Domanski, J. P. Correa-Baena, M. K. Nazeeruddin, S. M. Zakeeruddin, W. Tress, A. Abate, A. Hagfeldt and M. Grätzel, *Energy Environ. Sci.*, 2016, **9**, 1989–1997.
- 19 T. Singh and T. Miyasaka, *Adv. Energy Mater.*, 2018, **8**, 1–9.
- 20 D. P. McMeekin, G. Sadoughi, W. Rehman, G. E. Eperon, M. Saliba, M. T. Hörantner, A. Haghhighirad, N. Sakai, L. Korte, B. Rech, M. B. Johnston, L. M. Herz and H. J. Snaith, *Science*, 2016, **351**, 151–155.
- 21 S. Mabrouk, B. Bahrami, A. Gurung, K. M. Reza, N. Adhikari, A. Dubey, R. Pathak, S. Yang and Q. Qiao, *Sustainable Energy Fuels*, 2017, **1**, 2162–2171.
- 22 M. Abdi-Jalebi, M. I. Dar, A. Sadhanala, S. P. Senanayak, M. Franckevičius, N. Arora, Y. Hu, M. K. Nazeeruddin, S. M. Zakeeruddin, M. Grätzel and R. H. Friend, *Adv. Energy Mater.*, 2016, **6**, 1502472.
- 23 M. Abdi-Jalebi, Z. Andaji-Garmaroudi, S. Cacovich, C. Stavrakas, B. Philippe, J. M. Richter, M. Alsari, E. P. Booker,



E. M. Hutter, A. J. Pearson, S. Lilliu, T. J. Savenije, H. Rensmo, G. Divitini, C. Ducati, R. H. Friend and S. D. Stranks, *Nature*, 2018, **555**, 497–501.

24 M. Saliba, T. Matsui, K. Domanski, J.-Y. Seo, A. Ummadisingu, S. M. Zakeeruddin, J.-P. Correa-Baena, W. R. Tress, A. Abate, A. Hagfeldt and M. Grätzel, *Science*, 2016, **354**, 206–209.

25 M. Abdi-Jalebi, M. I. Dar, A. Sadhanala, S. P. Senanayak, M. Grätzel and R. H. Friend, *J. Vis. Exp.*, 2017, 1–9.

26 H. Lu, Y. Liu, P. Ahlawat, A. Mishra, W. R. Tress, F. T. Eickemeyer, Y. Yang, F. Fu, Z. Wang, C. E. Avalos, B. I. Carlsen, A. Agarwalla, X. Zhang, X. Li, Y. Zhan, S. M. Zakeeruddin, L. Emsley, U. Rothlisberger, L. Zheng, A. Hagfeldt and M. Grätzel, *Science*, 2020, **370**, 6512.

27 W. Hui, L. Chao, H. Lu, F. Xia, Q. Wei, Z. Su, T. Niu, L. Tao, B. Du, D. Li, Y. Wang, H. Dong, S. Zuo, B. Li, W. Shi, X. Ran, P. Li, H. Zhang, Z. Wu, C. Ran, L. Song, G. Xing, X. Gao, J. Zhang, Y. Xia, Y. Chen and W. Huang, *Science*, 2021, **371**, 1359–1364.

28 G. Kim, H. Min, K. S. Lee, D. Y. Lee, S. M. Yoon and S. il Seok, *Science*, 2020, **370**, 108–112.

29 H. Min, M. Kim, S. U. Lee, H. Kim, G. Kim, K. Choi, J. H. Lee and S. il Seok, *Science*, 2019, **366**, 749–753.

30 M. Kim, J. Jeong, H. Lu, T. K. Lee, F. T. Eickemeyer, Y. Liu, I. W. Choi, S. J. Choi, Y. Jo, H. B. Kim, S. I. Mo, Y. K. Kim, H. Lee, N. G. An, S. Cho, W. R. Tress, S. M. Zakeeruddin, A. Hagfeldt, J. Y. Kim, M. Grätzel and D. S. Kim, *Science*, 2022, **375**, 302–306.

31 T. A. S. Doherty, S. Nagane, D. J. Kubicki, Y. K. Jung, D. N. Johnstone, A. N. Iqbal, D. Guo, K. Frohma, M. Danaie, E. M. Tennyson, S. Macpherson, A. Abfalterer, M. Anaya, Y. H. Chiang, P. Crout, F. S. Ruggeri, S. M. Collins, C. P. Grey, A. Walsh, P. A. Midgley and S. D. Stranks, *Science*, 2021, **374**, 1598–1605.

32 J. W. Lee, S. Tan, S. il Seok, Y. Yang and N. G. Park, *Science*, 2022, **375**, 6583.

33 M. Saliba, T. Matsui, K. Domanski, J. Y. Seo, A. Ummadisingu, S. M. Zakeeruddin, J. P. Correa-Baena, W. R. Tress, A. Abate, A. Hagfeldt and M. Grätzel, *Science*, 2016, **354**, 206–209.

34 A. Y. Alsalloum, B. Turedi, X. Zheng, S. Mitra, A. A. Zhumekeenov, K. J. Lee, P. Maity, I. Gereige, A. AlSaggaf, I. S. Roqan, O. F. Mohammed and O. M. Bakr, *ACS Energy Lett.*, 2020, **5**, 657–662.

35 K. Wang, C. Wu, Y. Hou, D. Yang, T. Ye, J. Yoon, M. Sanghadasa and S. Priya, *Energy Environ. Sci.*, 2020, **13**, 3412–3422.

36 Q. Jiang, Y. Zhao, X. Zhang, X. Yang, Y. Chen, Z. Chu, Q. Ye, X. Li, Z. Yin and J. You, *Nat. Photonics*, 2019, **13**, 460–466.

37 Y. W. Jang, S. Lee, K. M. Yeom, K. Jeong, K. Choi, M. Choi and J. H. Noh, *Nat. Energy*, 2021, **6**(1), 63–71.

38 J. Peng, D. Walter, Y. Ren, M. Tebyetekerwa, Y. Wu, T. Duong, Q. Lin, J. Li, T. Lu, M. A. Mahmud, O. L. C. Lem, S. Zhao, W. Liu, Y. Liu, H. Shen, L. Li, F. Kremer, H. T. Nguyen, D. Y. Choi, K. J. Weber, K. R. Catchpole and T. P. White, *Science*, 2021, **371**, 390–395.

39 J. J. Yoo, G. Seo, M. R. Chua, T. G. Park, Y. Lu, F. Rotermund, Y. Kim, C. S. Moon, N. J. Jeon, V. Bulović, S. S. Shin and M. G. Bawendi, *Nature*, 2021, **590**, 587–593.

40 M. Jeong, I. W. Choi, E. M. Go, Y. Cho, M. Kim, B. Lee, S. Jeong, Y. Jo, H. W. Choi, J. Lee, J. H. Bae, S. K. Kwak, D. S. Kim and C. Yang, *Science*, 2020, **369**, 6511.

41 H. Min, D. Y. Lee, J. Kim, G. Kim, K. S. Lee, J. Kim, M. J. Paik, Y. K. Kim, K. S. Kim, M. G. Kim, T. J. Shin and S. il Seok, *Nature*, 2021, **598**, 444–450.

42 Z. Yi, N. H. Ladi, X. Shai, H. Li, Y. Shen and M. Wang, *Nanoscale Adv.*, 2019, **1**, 1276–1289.

43 J. Y. Kim, J. W. Lee, H. S. Jung, H. Shin and N. G. Park, *Chem. Rev.*, 2020, **120**, 7867–7918.

44 T. Chen, B. J. Foley, C. Park, C. M. Brown, L. W. Harriger, J. Lee, J. Ruff, M. Yoon, J. J. Choi and S. H. Lee, *Sci. Adv.*, 2016, **2**, 1–7.

45 N. Pellet, P. Gao, G. Gregori, T. Y. Yang, M. K. Nazeeruddin, J. Maier and M. Grätzel, *Angew. Chem., Int. Ed.*, 2014, **53**, 3151–3157.

46 A. Binek, F. C. Hanusch, P. Docampo and T. Bein, *J. Phys. Chem. Lett.*, 2015, **6**, 1249–1253.

47 X. Dong, L. Chao, T. Niu, Y. Li, P. Guo, W. Hui, L. Song, Z. Wu and Y. Chen, *Solar RRL*, 2022, **2200060**(6), 7.

48 N. J. Jeon, J. H. Noh, W. S. Yang, Y. C. Kim, S. Ryu, J. Seo and S. il Seok, *Nature*, 2015, **517**, 476–480.

49 Z. Li, M. Yang, J. S. Park, S. H. Wei, J. J. Berry and K. Zhu, *Chem. Mater.*, 2016, **28**, 284–292.

50 J. W. Lee, D. H. Kim, H. S. Kim, S. W. Seo, S. M. Cho and N. G. Park, *Adv. Energy Mater.*, 2015, **5**, 1501310.

51 X. Xia, W. Wu, H. Li, B. Zheng, Y. Xue, J. Xu, D. Zhang, C. Gao and X. Liu, *RSC Adv.*, 2016, **6**, 14792–14798.

52 Y. H. Park, I. Jeong, S. Bae, H. J. Son, P. Lee, J. Lee, C. H. Lee and M. J. Ko, *Adv. Funct. Mater.*, 2017, **27**, 1605988.

53 L. Zhang, W. Cui, Z. Zang, F. Tian, X. Li and G. Qin, *Solar Energy*, 2019, **188**, 224–229.

54 T. Duong, H. K. Mulmudi, H. Shen, Y. L. Wu, C. Barugkin, Y. O. Mayon, H. T. Nguyen, D. Macdonald, J. Peng, M. Lockrey, W. Li, Y. B. Cheng, T. P. White, K. Weber and K. Catchpole, *Nano Energy*, 2016, **30**, 330–340.

55 M. Zhang, J. S. Yun, Q. Ma, J. Zheng, C. F. J. Lau, X. Deng, J. Kim, D. Kim, J. Seidel, M. A. Green, S. Huang and A. W. Y. Ho-Baillie, *ACS Energy Lett.*, 2017, **2**, 438–444.

56 Y. Hu, M. F. Aygüler, M. L. Petrus, T. Bein and P. Docampo, *ACS Energy Lett.*, 2017, **2**, 2212–2218.

57 C. Yi, J. Luo, S. Meloni, A. Boziki, N. Ashari-Astani, C. Grätzel, S. M. Zakeeruddin, U. Röthlisberger and M. Grätzel, *Energy Environ. Sci.*, 2016, **9**, 656–662.

58 D. J. Kubicki, S. D. Stranks, C. P. Grey and L. Emsley, *Nat. Rev. Chem.*, 2021, **5**, 624–645.

59 L. Piveteau, V. Morad and M. V. Kovalenko, *J. Am. Chem. Soc.*, 2020, **142**, 19413–19437.

60 D. J. Kubicki, D. Prochowicz, A. Hofstetter, S. M. Zakeeruddin, M. Grätzel and L. Emsley, *J. Am. Chem. Soc.*, 2017, **139**, 14173–14180.

61 D. J. Kubicki, D. Prochowicz, A. Hofstetter, S. M. Zakeeruddin, M. Grätzel and L. Emsley, *J. Am. Chem. Soc.*, 2018, **140**(23), 7232–7238.

62 Y. Hu, M. F. Aygüler, M. L. Petrus, T. Bein and P. Docampo, *ACS Energy Lett.*, 2017, **2**, 2212–2218.

63 M. Abdi-Jalebi, Z. Andaji-Garmaroudi, A. J. Pearson, G. Divitini, S. Cacovich, B. Philippe, H. Rensmo, C. Ducati, R. H. Friend and S. D. Stranks, *ACS Energy Lett.*, 2018, **3**, 2671–2678.

64 A. Mishra, D. J. Kubicki, A. Boziki, R. D. Chavan, M. Dankl, M. Mladenović, D. Prochowicz, C. P. Grey, U. Rothlisberger and L. Emsley, *ACS Energy Lett.*, 2022, **7**, 2745–2752.

65 O. J. Usiobo, H. Kanda, P. Gratia, I. Zimmermann, T. Wirtz, M. K. Nazeeruddin and J. N. Audinot, *J. Phys. Chem. C*, 2020, **124**, 23230–23236.

66 D. Y. Son, S. G. Kim, J. Y. Seo, S. H. Lee, H. Shin, D. Lee and N. G. Park, *J. Am. Chem. Soc.*, 2018, **140**, 1358–1364.

67 Z. Andaji-Garmaroudi, M. Anaya, A. J. Pearson and S. D. Stranks, *Adv. Energy Mater.*, 2020, **10**, 1903109.

68 T. A. S. Doherty, A. J. Winchester, S. Macpherson, D. N. Johnstone, V. Pareek, E. M. Tennyson, S. Kosar, F. U. Kosasih, M. Anaya, M. Abdi-Jalebi, Z. Andaji-Garmaroudi, E. L. Wong, J. Madéo, Y. H. Chiang, J. S. Park, Y. K. Jung, C. E. Petoukhoff, G. Divitini, M. K. L. Man, C. Ducati, A. Walsh, P. A. Midgley, K. M. Dani and S. D. Stranks, *Nature*, 2020, **580**, 360–366.

69 S. Macpherson, T. A. S. Doherty, A. J. Winchester, S. Kosar, D. N. Johnstone, Y.-H. Chiang, K. Galkowski, M. Anaya, K. Frohna, A. N. Iqbal, S. Nagane, B. Roose, Z. Andaji-Garmaroudi, K. W. P. Orr, J. E. Parker, P. A. Midgley, K. M. Dani and S. D. Stranks, *Nature*, 2022, **2022**, 1–3.

70 M. P. Hanrahan, L. Men, B. A. Rosales, J. Vela and A. J. Rossini, *Chem. Mater.*, 2018, **30**, 7005–7015.

71 A. J. Rossini, A. Zagdoun, M. Lelli, A. Lesage, C. Copéret and L. Emsley, *Acc. Chem. Res.*, 2013, **46**, 1942–1951.

72 B. A. Rosales, M. P. Hanrahan, B. W. Boote, A. J. Rossini, E. A. Smith and J. Vela, *ACS Energy Lett.*, 2017, **2**, 906–914.

73 A. Mishra, M. A. Hope, M. Almalki, L. Pfeifer, S. M. Zakeeruddin, M. Grätzel and L. Emsley, *J. Am. Chem. Soc.*, 2022, **144**, 15175–15184.

74 Q. Huang, Y. Zou, S. A. Bourelle, T. Zhai, T. Wu, Y. Tan, Y. Li, J. Li, S. Duhm, T. Song, L. Wang, F. Deschler and B. Sun, *Nanoscale Horiz.*, 2019, **4**, 924–932.

75 F. Yang, M. A. Kamarudin, G. Kapil, D. Hirotani, P. Zhang, C. H. Ng, T. Ma and S. Hayase, *ACS Appl. Mater. Interfaces*, 2018, **10**, 24543–24548.

76 T. J. Jacobsson, M. Pazoki, A. Hagfeldt and T. Edvinsson, *J. Phys. Chem. C*, 2015, **119**, 25673–25683.

77 J. Navas, A. Sánchez-Coronilla, J. J. Gallardo, N. Cruz Hernández, J. C. Piñero, R. Alcántara, C. Fernández-Lorenzo, D. M. de Los Santos, T. Aguilar and J. Martín-Calleja, *Nanoscale*, 2015, **7**, 6216–6229.

78 N. Phung, R. Félix, D. Meggiolaro, A. Al-Ashouri, G. Sousa, E. Silva, C. Hartmann, J. Hidalgo, H. Köbler, E. Mosconi, B. Lai, R. Gunder, M. Li, K. L. Wang, Z. K. Wang, K. Nie, E. Handick, R. G. Wilks, J. A. Marquez, B. Rech, T. Unold, J. P. Correa-Baena, S. Albrecht, F. de Angelis, M. Bär and A. Abate, *J. Am. Chem. Soc.*, 2020, **142**, 2364–2374.

79 D. J. Kubicki, D. Prochowicz, A. Hofstetter, S. M. Zakeeruddin, M. Grätzel and L. Emsley, *J. Am. Chem. Soc.*, 2017, **139**, 14173–14180.

80 D. J. Kubicki, D. Prochowicz, A. Hofstetter, S. M. Zakeeruddin, M. Grätzel and L. Emsley, *J. Am. Chem. Soc.*, 2018, **140**, 7232–7238.

81 P. Zhao, W. Yin, M. Kim, M. Han, Y. J. Song, T. K. Ahn and H. S. Jung, *J. Mater. Chem. A*, 2017, **5**, 7905–7911.

82 Z. Tang, T. Bessho, F. Awai, T. Kinoshita, M. M. Maitani, R. Jono, T. N. Murakami, H. Wang, T. Kubo, S. Uchida and H. Segawa, *Sci. Rep.*, 2017, **7**, 12183.

83 D.-Y. Son, S.-G. Kim, J.-Y. Seo, S.-H. Lee, H. Shin, D. Lee and N.-G. Park, *J. Am. Chem. Soc.*, 2018, **140**(4), 1358–1364.

84 T. Bu, X. Liu, Y. Zhou, J. Yi, X. Huang, L. Luo, J. Xiao, Z. Ku, Y. Peng, F. Huang, Y. B. Cheng and J. Zhong, *Energy Environ. Sci.*, 2017, **10**, 2509–2515.

85 J. K. Nam, S. U. Chai, W. Cha, Y. J. Choi, W. Kim, M. S. Jung, J. Kwon, D. Kim and J. H. Park, *Nano Lett.*, 2017, **17**, 2028–2033.

86 W. Shockley and H. J. Queisser, *J. Appl. Phys.*, 1961, **32**, 510.

87 S. Meloni, G. Palermo, N. Ashari-Astani, M. Grätzel and U. Rothlisberger, *J. Mater. Chem. A*, 2016, **4**, 15997–16002.

88 M. R. Filip, G. E. Eperon, H. J. Snaith and F. Giustino, *Nat. Commun.*, 2014, **5**(1), 1–9.

89 H. Choi, J. Jeong, H. B. Kim, S. Kim, B. Walker, G. H. Kim and J. Y. Kim, *Nano Energy*, 2014, **7**, 80–85.

90 Z. Liu, P. Liu, M. Li, T. He, T. Liu, L. Yu and M. Yuan, *Adv. Energy Mater.*, 2022, **2200111**, 1–35.

91 O. A. Syzgantseva, M. Saliba, M. Grätzel and U. Rothlisberger, *J. Phys. Chem. Lett.*, 2017, **8**, 1191–1196.

92 T. Jesper Jacobsson, J. P. Correa-Baena, M. Pazoki, M. Saliba, K. Schenk, M. Grätzel and A. Hagfeldt, *Energy Environ. Sci.*, 2016, **9**, 1706–1724.

93 R. Prasanna, A. Gold-Parker, T. Leijtens, B. Conings, A. Babayigit, H. G. Boyen, M. F. Toney and M. D. McGehee, *J. Am. Chem. Soc.*, 2017, **139**, 11117–11124.

94 H. Tsai, W. Nie, J. C. Blancon, C. C. Stoumpos, R. Asadpour, B. Harutyunyan, A. J. Neukirch, R. Verduzco, J. J. Crochet, S. Tretiak, L. Pedesseau, J. Even, M. A. Alam, G. Gupta, J. Lou, P. M. Ajayan, M. J. Bedzyk, M. G. Kanatzidis and A. D. Mohite, *Nature*, 2016, **536**, 312–317.

95 F. Zhang, H. Lu, J. Tong, J. J. Berry, M. C. Beard and K. Zhu, *Energy Environ. Sci.*, 2020, **13**, 1154–1186.

96 Y. Liu, S. Akin, A. Hinderhofer, F. T. Eickemeyer, H. Zhu, J. Y. Seo, J. Zhang, F. Schreiber, H. Zhang, S. M. Zakeeruddin, A. Hagfeldt, M. I. Dar and M. Grätzel, *Angew. Chem., Int. Ed.*, 2020, **59**, 15688–15694.

97 J. W. Lee, Z. Dai, T. H. Han, C. Choi, S. Y. Chang, S. J. Lee, N. de Marco, H. Zhao, P. Sun, Y. Huang and Y. Yang, *Nat. Commun.*, 2018, **9**, 1–10.

98 N. Li, Z. Zhu, C. C. Chueh, H. Liu, B. Peng, A. Petrone, X. Li, L. Wang and A. K. Y. Jen, *Adv. Energy Mater.*, 2017, **7**, 1–9.

99 P. Yadav, M. H. Alotaibi, N. Arora, M. I. Dar, S. M. Zakeeruddin and M. Grätzel, *Adv. Funct. Mater.*, 2018, **28**, 1–7.

100 G. Xing, N. Mathews, S. Sun, S. S. Lim, Y. M. Lam, M. Gratzel, S. Mhaisalkar and T. C. Sum, *Science*, 2013, **342**, 344–347.

101 G. E. Eperon, S. D. Stranks, C. Menelaou, M. B. Johnston, L. M. Herz and H. J. Snaith, *Energy Environ. Sci.*, 2014, **7**, 982–988.

102 D. J. Kubicki, D. Prochowicz, A. Hofstetter, M. Saski, P. Yadav, D. Bi, N. Pellet, J. Lewiński, S. M. Zakeeruddin, M. Grätzel and L. Emsley, *J. Am. Chem. Soc.*, 2018, **140**, 3345–3351.

103 D. H. Fabini, T. A. Siaw, C. C. Stoumpos, G. Laurita, D. Olds, K. Page, J. G. Hu, M. G. Kanatzidis, S. Han and R. Seshadri, *J. Am. Chem. Soc.*, 2017, **139**, 16875–16884.

104 F. Ambrosio, J. Wiktor, F. de Angelis and A. Pasquarello, *Energy Environ. Sci.*, 2018, **11**, 101–105.

105 J. Wiktor, F. Ambrosio and A. Pasquarello, *J. Mater. Chem. A*, 2018, **6**, 16863–16867.

106 S. Feldmann, S. Macpherson, S. P. Senanayak, M. Abdi-Jalebi, J. P. H. Rivett, G. Nan, G. D. Tainter, T. A. S. Doherty, K. Frohna, E. Ringe, R. H. Friend, H. Sirringhaus, M. Saliba, D. Beljonne, S. D. Stranks and F. Deschler, *Nat. Photonics*, 2020, **14**, 123–128.

107 M. Ledinsky, A. Vlk, T. Schonfeldova, J. Holovsky, E. Aydin, H. X. Dang, Z. Hajkova, L. Landova, J. Valenta, A. Fejfar and S. de Wolf, *J. Phys. Chem. C*, 2020, **124**, 27333–27339.

108 J. H. Noh, S. H. Im, J. H. Heo, T. N. Mandal and S. il Seok, *Nano Lett.*, 2013, **13**, 1764–1769.

109 B. Philippe, M. Saliba, J. P. Correa-Baena, U. B. Cappel, S. H. Turren-Cruz, M. Grätzel, A. Hagfeldt and H. Rensmo, *Chem. Mater.*, 2017, **29**, 3589–3596.

110 A. Solanki, P. Yadav, S. H. Turren-Cruz, S. S. Lim, M. Saliba and T. C. Sum, *Nano Energy*, 2019, **58**, 604–611.

111 S. Cacovich, F. Matteocci, M. Abdi-Jalebi, S. D. Stranks, A. di Carlo, C. Ducati and G. Divitini, *ACS Appl. Energy Mater.*, 2018, **1**, 7174–7181.

112 S. D. Stranks, *ACS Energy Lett.*, 2017, **2**, 1515–1525.

113 D. M. Trots and S. v Myagkota, *J. Phys. Chem. Solids*, 2008, **69**, 2520–2526.

114 E. Mosconi and F. de Angelis, *ACS Energy Lett.*, 2016, **1**, 182–188.

115 A. Senocrate, T. Acartürk, G. Y. Kim, R. Merkle, U. Starke, M. Grätzel and J. Maier, *J. Mater. Chem. A*, 2018, **6**, 10847–10855.

116 D. Lin, T. Shi, H. Xie, F. Wan, X. Ren, K. Liu, Y. Zhao, L. Ke, Y. Lin, Y. Gao, X. Xu, W. Xie, P. Liu and Y. Yuan, *Adv. Energy Mater.*, 2021, **11**, 1–8.

117 Y. Yuan and J. Huang, *Acc. Chem. Res.*, 2016, **49**, 286–293.

118 S. Tan, I. Yavuz, N. de Marco, T. Huang, S. J. Lee, C. S. Choi, M. Wang, S. Nuryyeva, R. Wang, Y. Zhao, H. C. Wang, T. H. Han, B. Dunn, Y. Huang, J. W. Lee and Y. Yang, *Adv. Mater.*, 2020, **32**, 1–11.

119 T. I. Alanazi, O. S. Game, J. A. Smith, R. C. Kilbride, C. Greenland, R. Jayaprakash, K. Georgiou, N. J. Terrill and D. G. Lidzey, *RSC Adv.*, 2020, **10**, 40341–40350.

120 D. Y. Son, S. G. Kim, J. Y. Seo, S. H. Lee, H. Shin, D. Lee and N. G. Park, *J. Am. Chem. Soc.*, 2018, **140**, 1358–1364.

121 L. Qiao, W.-H. Fang, R. Long and O. V. Prezhdo, *Angew. Chem.*, 2020, **132**, 4714–4720.

122 M. Kim, G. H. Kim, T. K. Lee, I. W. Choi, H. W. Choi, Y. Jo, Y. J. Yoon, J. W. Kim, J. Lee, D. Huh, H. Lee, S. K. Kwak, J. Y. Kim and D. S. Kim, *Joule*, 2019, **3**, 2179–2192.

123 C. Mu, J. Pan, S. Feng, Q. Li and D. Xu, *Adv. Energy Mater.*, 2017, **7**, 3–8.

124 B. Wook Park, H. W. Kwon, Y. Lee, D. Y. Lee, M. G. Kim, G. Kim, K. Jeong Kim, Y. K. Kim, J. Im, T. J. Shin and S. Il Seok, *Nat. Energy*, 2021, **6**(4), 419–428.

125 W. S. Yang, J. H. Noh, N. J. Jeon, Y. C. Kim, S. Ryu, J. Seo and S. il Seok, *Science*, 2015, **348**, 1234–1237.

126 J. W. Lee, Z. Dai, C. Lee, H. M. Lee, T. H. Han, N. de Marco, O. Lin, C. S. Choi, B. Dunn, J. Koh, D. di Carlo, J. H. Ko, H. D. Maynard and Y. Yang, *J. Am. Chem. Soc.*, 2018, **140**, 6317–6324.

127 J. W. Lee, H. S. Kim and N. G. Park, *Acc. Chem. Res.*, 2016, **49**, 311–319.

128 F. Wang, W. Geng, Y. Zhou, H. H. Fang, C. J. Tong, M. A. Loi, L. M. Liu and N. Zhao, *Adv. Mater.*, 2016, **28**, 9986–9992.

129 K. M. M. Salim, S. Masi, A. F. Gualdrón-Reyes, R. S. Sánchez, E. M. Barea, M. Krećmarová, J. F. Sánchez-Royo and I. Mora-Seró, *ACS Energy Lett.*, 2021, **6**, 3511–3521.

130 T. Niu, J. Lu, M. C. Tang, D. Barrit, D. M. Smilgies, Z. Yang, J. Li, Y. Fan, T. Luo, I. McCulloch, A. Amassian, S. Liu and K. Zhao, *Energy Environ. Sci.*, 2018, **11**, 3358–3366.

131 G. Wang, L. Wang, J. Qiu, Z. Yan, K. Tai, W. Yu and X. Jiang, *Solar Energy*, 2019, **187**, 147–155.

132 Y. Liu, S. Akin, L. Pan, R. Uchida, N. Arora, J. V. Milić, A. Hinderhofer, F. Schreiber, A. R. Uhl, S. M. Zakeeruddin, A. Hagfeldt, M. Ibrahim Dar and M. Grätzel, *Sci. Adv.*, 2019, **5**, 1–9.

133 Y. Zhang, S. G. Kim, D. K. Lee and N. G. Park, *Chem-SusChem*, 2018, **11**, 1813–1823.

134 H. Chen, Y. Chen, T. Zhang, X. Liu, X. Wang and Y. Zhao, *Small Struct.*, 2021, **2**, 2000130.

135 M. I. Saidaminov, A. L. Abdelhady, G. Maculan and O. M. Bakr, *Chem. Commun.*, 2015, **51**, 17658–17661.

136 D. Prochowicz, P. Yadav, M. Saliba, D. J. Kubicki, M. M. Tavakoli, S. M. Zakeeruddin, J. Lewiński, L. Emsley and M. Grätzel, *Nano Energy*, 2018, **49**, 523–528.

137 D. Prochowicz, P. Yadav, M. Saliba, M. Saski, S. M. Zakeeruddin, J. Lewiński and M. Grätzel, *ACS Appl. Mater. Interfaces*, 2017, **9**, 28418–28425.

138 F. Wang, H. Yu, H. Xu and N. Zhao, *Adv. Funct. Mater.*, 2015, **25**, 1120–1126.

139 G. Li, T. Zhang, F. Xu and Y. Zhao, *Mater. Today Energy*, 2017, **5**, 293–298.

140 M. Kim, G. H. Kim, K. S. Oh, Y. Jo, H. Yoon, K. H. Kim, H. Lee, J. Y. Kim and D. S. Kim, *ACS Nano*, 2017, **11**, 6057–6064.

141 C. Zhu, X. Niu, Y. Fu, N. Li, C. Hu, Y. Chen, X. He, G. Na, P. Liu, H. Zai, Y. Ge, Y. Lu, X. Ke, Y. Bai, S. Yang, P. Chen, Y. Li, M. Sui, L. Zhang, H. Zhou and Q. Chen, *Nat. Commun.*, 2019, **10**(1), 1–11.

142 T. A. S. Doherty, S. Nagane, D. J. Kubicki, Y. K. Jung, D. N. Johnstone, A. N. Iqbal, D. Guo, K. Frohna,



M. Danaie, E. M. Tennyson, S. Macpherson, A. Abfalterer, M. Anaya, Y. H. Chiang, P. Crout, F. S. Ruggeri, S. M. Collins, C. P. Grey, A. Walsh, P. A. Midgley and S. D. Stranks, *Science*, 2021, **374**, 1598–1605.

143 M. C. Tang, Y. Fan, D. Barrit, X. Chang, H. X. Dang, R. Li, K. Wang, D. M. Smilgies, S. F. Liu, S. de Wolf, T. D. Anthopoulos, K. Zhao and A. Amassian, *J. Mater. Chem. A*, 2020, **8**, 1095–1104.

144 C. Chen, J. Chen, H. Han, L. Chao, J. Hu, T. Niu, H. Dong, S. Yang, Y. Xia, Y. Chen and W. Huang, *Nature*, 2022, **2022**, 1–6.

145 R. Patidar, D. Burkitt, K. Hooper, D. Richards and T. Watson, *Mater. Today Commun.*, 2020, **22**, 100808.

146 Z. Li, P. Li, G. Chen, Y. Cheng, X. Pi, X. Yu, D. Yang, L. Han, Y. Zhang and Y. Song, *ACS Appl. Mater. Interfaces*, 2020, **12**, 39082–39091.